Current Pollution Reports (2023) 9:486–509
https://doi.org/10.1007/s40726-023-00264-9

Acoustic Beamforming Algorithms and Their Applications in Environmental Noise

Gaetano Licitra[1,2] · Francesco Artuso[3] · Marco Bernardini[4] · Antonino Moro[5] · Francesco Fidecaro[3] · Luca Fredianelli[2]

Accepted: 23 April 2023 / Published online: 31 May 2023

Abstract

Purpose of Review Rather than broadly investigating the beamforming field, the present work has the distinctive feature of analyzing the most common algorithms through both a theoretical presentation and a report of their most recent applications to real cases. The intent is to take a step forward towards the harmonization of the sector with a combined approach that could prove to be useful for academics willing to understand the theory and for technicians needing to choose the best algorithms to use in different measurement conditions.

Recent Findings In recent years, the sector has seen the growth of studies published on the use of beamforming techniques and their applications to real cases. Unfortunately, different authors and research groups developed so many different algorithms that a literature review turns out to be essential to increase awareness and to avoid confusion for both scientists and technicians.

Summary Nowadays, acoustic cameras have been proven to be powerful instruments that combine a video acquisition with a microphone array to obtain real-time information about the location of noise sources. Different beamforming techniques can be applied to sound signals allowing their visualization or distinguishing the contribution of multiple different emitters. This quality, historically used in different branches of acoustics, is now spreading into environmental noise protection, especially where it is needed to locate the emitters or to better study sources that have not yet been characterized. Acoustic cameras can also be used to identify the responsible for noise limits exceedings at receivers when traditional microphone measurements are not enough, or to identify potential leakages occurred in the installation of noise abatement measurements.

Keywords Beamforming · Acoustic camera · Beamforming applications · Beamforming algorithms · Environmental noise · Sound source localization

Introduction

A microphone array is a device made of a set of microphones which record sound pressure simultaneously, for the subsequent computation of the arrival angle of sound, made through algorithms based on beamforming techniques. Firstly used in 1976 [1] for studying the noise emitted by a turbojet engine, microphone arrays have nowadays evolved into acoustic camera (AC), a tool that can directly apply beamforming to the signals acquired

✉ Gaetano Licitra
g.licitra@arpat.toscana.it

✉ Luca Fredianelli
luca.fredianelli@ipcf.cnr.it

Francesco Artuso
francesco.artuso@phd.unipi.it

Marco Bernardini
marcobernardini.s@gmail.com

Antonino Moro
antonino.moro@i-pool.it

Francesco Fidecaro
francesco.fidecaro@unipi.it

[1] Environmental Protection Agency of Tuscany Region, Via Vittorio Veneto 27, Pisa 56127, Italy

[2] Institute of Chemical and Physical Processes of National Research Council, Via G. Moruzzi 1, Pisa 56124, Italy

[3] Physics Department, University of Pisa, Largo Bruno Pontecorvo 3, 56127 Pisa, Italy

[4] Section of Acoustics and Sensors O.M. Corbino, CNR-INM, Via del Fosso del Cavaliere 100, 00133 Rome, Italy

[5] iPOOL S.r.l., Via Cocchi 7, Pisa 56121, Italy

with many microphones. The fast development10 of computationally efficient units played an important role in the evolution of ACs, allowing to process bigger quantities of data in a shorter period, even reaching real-time speed for some algorithms. On the other hand, stronger computational capability also allowed to use more complex and accurate algorithms without significant increase in the computing time. This led to the possibility of increasing the sampling frequency and the number of microphones in the arrays and improving the resolution [2]. Many companies can now produce ACs, with arrays of different sizes, shapes, and numbers of microphones. An open source software in python language [3] that allows to perform beamforming on raw data acquired with custom arrays confirms the spread of this technique. The advancement and commercialization of beamforming techniques involved many different on-field applications in environmental acoustics and AC turned out to be very useful in complex scenarios. Among all, AC are useful when conventional measurements of sound pressure level are not sufficient to characterize a source and when it is difficult to localize the principal noise source among many others. Also, sound leakage investigation [4, 5] and other indoor measurements [6] can benefit from ACs. Many kinds of noise sources have been now investigated with beamforming, such as high-speed trains [7], cars in motion [8, 9], flying aircrafts [10–12], helicopters [13], wind turbines [14, 15], unmanned aerial vehicle [16], industries [17–20], ports [21, 22], and urban environment [23, 24]. Modern frontiers see acoustic beamforming combined with machine learning, with tests performed in various applications [25–28].

In this complex and fast developing field of study, many different algorithms have emerged and both academics and professionals may wish to easy access the up-to-date informations. The present paper reviews the state-of-the-art on the main beamforming algorithms used in direction of arrival (DOA) estimation from both theoretical and application points of view. The theoretical part is expected to be interesting for readers and scientists looking for a first collection of the methods. The applications can be interesting for professionals willing to investigate what algorithm is used in different measurement conditions. Advantages and disadvantages of each algorithm in different applications are reported according to what found in literature. Moreover, a side goal of the present work is to find similarities among the multitude of algorithms and to highlight the differences. Aspects around acoustic cameras have been already reviewed in the past. In particular, Leclére et al. [29•], Chiariotti et al. [30•], and Merino-Martínez et al. [31•] altogether showed an historical overview of beamforming, the key concepts of the problem, the criteria which guide the experimental setup and procedure, the beamforming approaches in general, some numerical simulations to test different methods in different scenarios, and, in the end, an overview of general applications. Since the publication of the last review in 2019, there has been a surge in publications with more than 175 papers (source *Scopus*) on acoustic beamforming algorithms, excluding ultrasounds and photoacoustics. However, the demand for an updated work is not only justified by recent numbers, but also because the previous reviews treat the beamforming field from a general point of view, while the present review is algorithm-oriented. The different approach is visible in both the theoretical and practical parts. Previous theoretical treatments explain the general idea behind beamforming and the mathematical principles of different beamforming macro-categories, while the present work analyzes each algorithm individually. For maximum clarity, the present review reports in details all the mathematical steps of every algorithm. Even if documents treating algorithms individually may exist in technical literature, they are not easy to find in scientific literature. Moreover, a single document collecting the mathematical proofs of many beamforming algorithms may represent a novelty and a convenience for readers. From an application point of view, the difference is straightforward, because the previous reviews collect general beamforming applications, while the present review analyzes real-case applications grouped by algorithm.

The paper is organized as follows. In the "Mathematical Formulations of Beamforming Algorithms" section, the mathematical formulations of the different algorithms are shown individually, while in the "On-Field Applications" section, the most recent applications found in literature, divided by algorithm, are reported and discussed in order to understand their potentials and limits. Finally, the "Discussion and Conclusions" section collects comparisons and discussion, final comments, and conclusive considerations about beamforming techniques. The basic theoretical concepts of beamforming are introduced in the Appendix section in order not to complicate the treatment. The paper is mainly divided in two self standing sections, and each algorithm is described without connection to the others, in order to allow readers interested only to particular algorithms to easily navigate in the document. However, the combination of both approaches allows a deeper understanding on how acoustic beamforming works. The knowledge of the mathematical formulations is an essential preliminary information to forecast how an algorithm may perform in different situations, but its applications in real scenarios may show unexpected behaviors.

Mathematical Formulations of Beamforming Algorithms

Various mathematical procedures have been developed and applied in order to extrapolate the arrival angle of sounds. By means of these algorithms, it is possible to associate an

acoustic strength to every point framed by the camera. At the end, the AC produces an intensity map as function of incident angle, which is overlapped to an image taken by an optical camera at the same time, specifying the distance from the source to the camera, to transform angles into position. The presence of a source implies, besides the presence of a main lobe in the acoustic map, also the existence of secondary lobes due to reflections or diffractions, which appear as fake sources. Complexity in the direction of arrival (DOA) estimation is given by these fake sources that may occur during measurements, and this is the reason why sophisticated algorithms are needed and have been developed over time. In order to produce a cleaner and more reliable acoustic map, an algorithm should be able to distinguish between real and fake sources. This implies having high spatial resolution, defined by the width of the main lobe when the intensity level drops of 3 dB relative to the peak, and high dynamic range, which is the difference between the peak level and the highest sidelobe level of beam pattern.

The present section reports the theoretical description of the most used beamforming algorithms currently used in DOA estimation, retrieved in the scientific literature, and reformulated in order to provide a uniform description. At this point, it is worth mentioning that the fundamental tool in beamforming procedure is the cross-spectral matrix (CSM) which describes the correlation between signals coming from the different microphones of the array. The basic theoretical treatment of general beamforming is not the subject of this work, and reference is made to specific texts such as Allen et al. [32]. However, for the reader's convenience and understanding of this section, a summary of the basic concepts is provided in the Appendix section.

The algorithms investigated in the paper belong to six macro-categories:

1. Conventional beamforming
2. Functional beamforming
3. Adaptive beamforming
4. Eigenvalue decomposition
5. Deconvolution methods
6. Holographic methods

The algorithm based on conventional beamforming that will be presented is Delay and Sum, which relies on the simple idea of exploiting delays of arrival of the plane wave over the different microphones to identify the source position. A step forward is taken with the functional beamforming approach. In fact, in this approach, the CSM is mathematically manipulated before computing DOA, differently from conventional beamforming. This step allows sidelobe suppression. Steering vectors are fixed in conventional beamforming, while the adaptive beamforming algorithms, for example Capon, foresee to optimize the choice of these vectors adapting it to the specific situation under analysis. Another interesting approach to the subject is represented by MUSIC algorithm which is based on the eigenvalue decomposition of the CSM. Manipulating the respective eigenvectors, it is possible to estimate the DOA. The group of advanced methods, called deconvolution methods, is rather different. The complexity of the later typology of algorithms, which includes the algorithms CLEAN-SC and DAMAS, is higher, because they are based on the post-processing of a preliminary acoustic map obtained with conventional methods. In this post-processing step, the map is cleaned up from fake sources, thus leaving only the real ones. The last group of algorithms, holographic methods, which includes the algorithm SONAH, relies on the theory of representing the sound pressure field as a linear combination of an orthonormal set of eigenfunctions. The aim of holographic methods is to obtain the coefficients of this linear combination, which allows to reproduce the sound pressure in every point of picture in the best way. Unfortunately, information about EigenValue-Optimized Beamforming (EVOB) algorithm cannot be retrieved neither from a theoretical nor an experimental point of view, as it is propriety of a specific acoustic camera manufacturing company. This algorithm was designed starting from the functional beamforming, but consistent original parts were added by the company. For the same reasons, also, its applications cannot be found and its use is not widespread in the scientific community.

Delay and Sum

Delay and Sum (DAS), also called conventional beamforming, is the basic and original beamforming algorithm [30•]. Consider the situation in which an array of M microphones is used to look for the DOA of the sound. The plane framed by the camera, which is parallel to the coplanar array of microphones, is divided in P control points, each one identified by an angle and a distance. It is needed only one angle to identify a control point because of the implicit assumption of sound plane waves due to sources which are far enough. The other angle is fixed because the control points lay on a plane parallel to the plane of the microphone array. For each one of these points, the DAS algorithm computes the following expression

$$bf(\vec{x}_p, t) = \frac{1}{M} \sum_{m=1}^{M} w_m \, A_m(\vec{x}_p, \vec{x}_m) \, p_m\left(t - \frac{|\vec{x}_p - \vec{x}_m|}{c}\right) \qquad (1)$$

where

- w_m is a weighting factor for the m^{th} microphone, used to optimize the overall outcome; conventional beamforming algorithms have sensor weights fixed, different from adaptive beamforming which adapts sensor weights to the situation under investigation.

- $A_m(\vec{x}_p, \vec{x}_m)$ is a scaling factor which takes into account the amplitude damping due to the distance between source and microphone, i.e., $A_m(\vec{x}_p, \vec{x}_m) = 4\pi||\vec{x}_p - \vec{x}_m||$.
- p_m is the pressure signal measured by the m^{th} microphone; note that it is delayed by a factor $\frac{|\vec{x}_p - \vec{x}_m|}{c}$.
- c is the wave propagation speed in the medium.

For every control point $\vec{x}_p$, the signal measured by each microphone is multiplied by two factors, $A_m(\vec{x}_p, \vec{x}_m)$ and w_m, which, respectively, account for the damping of the wave amplitude due to the source-microphone distance and implement an optimization procedure. Furthermore, the array is "steered" towards $\vec{x}_p$ direction by means of the delay inserted in the pressure signal. At this point, it is computed the mean of these M reconstructed signals, which gives rise to $bf(\vec{x}_p, t)$, the outcome of the DAS algorithm. For every control point $\vec{x}_p$, the quantity $bf(\vec{x}_p, t)$ is computed.

If the control point under investigation $\vec{x}_p$ contains a source, then the M reconstructed signals will turn out to be in phase and each one at its maximum amplitude, so that the outcome $bf(\vec{x}_p, t)$ will be maximum, while if the control point $\vec{x}_p$ does not contain any source, the outcome $bf(\vec{x}_p, t)$ will be lower. In other words, delays allow constructive interference from particular angles and destructive interference from the others. Therefore, in the practical implementation of the procedure, the control points are scanned and the outcome $bf(\vec{x}_p, t)$ for every $\vec{x}_p$ is computed and recorded. In this way, a map of amplitudes is built and the source position is estimated as the control points which give rise to the maximum values of $bf(\vec{x}_p, t)$.

In the frequency domain the DAS formulation is equal to

$$bf(\vec{x}_p, \omega_k) = \frac{1}{M} \sum_{m=1}^{M} w_m \, A_m(\vec{x}_p, \vec{x}_m) \, P_m(\omega_k) e^{j\omega_k \Delta_{p,m}} \tag{2}$$

where

- $P_m(\omega_k)$ is the pressure signal at the m^{th} microphone and at the angular frequency ω_k
- $e^{j\omega_k \Delta_{p,m}}$ is the phase shift used to "steer" the array towards the $\vec{x}_p$ direction
- $\Delta_{p,m}$ is equal to $\frac{|\vec{x}_p - \vec{x}_m|}{c}$

Functional Beamforming

Functional beamforming (FB) is an improvement of conventional beamforming that was firstly developed by Dougherty in 2014 [33, 34]. As already said, conventional beamforming methods identify the location of the source using the phase delays between the emitted sound signal at the source and the received signals at each microphone in the array. Functional beamforming obtains an expression for the source autopower that benefits the real positions of the sources and disadvantages of other positions where sidelobes may take place. From a mathematical point of view, the starting point is the CSM:

$$\mathbf{C} = \frac{1}{2}\mathbf{p}\mathbf{p}^* = \mathbf{U}\mathbf{\Sigma}\mathbf{U}^* \tag{3}$$

where $\mathbf{p}$ and $\mathbf{p}^*$ are, respectively, the vector containing the Fourier transform of the recorded pressure amplitudes for each microphone at a frequency f and its conjugate transpose. In the following step, the eigenvalue decomposition of the CSM has been performed. Indeed, U is a unitary matrix whose columns are the CSM eigenvectors, while Σ is a diagonal matrix whose diagonal elements are the eigenvalues of the CSM. The steering vectors are defined as:

$$g_{j,n} = \frac{-exp(-2\pi i f \Delta t_{j,n})}{4\pi||\mathbf{x}_n - \boldsymbol{\xi}_j||(1 - ||\mathbf{M}||cos(\theta))^2} \tag{4}$$

where $\mathbf{M}$ is the Mach number, which is equal to the fraction between the velocity vector of the source and the sound speed, namely $\mathbf{M} = \mathbf{V}/c$. The general estimate for the source autopower at grid point position ξ_j is:

$$A_v(\xi_j) = \mathbf{w}_j^* \mathbf{C} \mathbf{w}_j \tag{5}$$

where the normalized steering vector is:

$$\mathbf{w}_j = \frac{\mathbf{g}_j}{||\mathbf{g}_j||^2} \tag{6}$$

In the formulation of the functional beamforming, Eq. (5) is modified using an exponent ν, whose value is chosen by the operator, in a way that will be shown in the following lines. The correct choice of this exponent ensures the best quality of the image. The source autopower for functional beamforming is:

$$A_v(\xi_j) = [\mathbf{w}_j^* \mathbf{C}^{\frac{1}{\nu}} \mathbf{w}_j]^\nu \tag{7}$$

In the case of a single source in position ξ_k, the dominant eigenvalue of the CSM is $s_k^2/2$ with the corresponding eigenvector g_k. Therefore, in this simplified case of a single source, using Eqs. (3) and (6) in Eq. (5), the autopower for a general location ξ_j is equal to:

$$A_v(\xi_j) = [\mathbf{w}_j^* \mathbf{C}^{\frac{1}{\nu}} \mathbf{w}_j]^\nu = \left[\frac{\mathbf{g}_j^* (\frac{1}{2} s_k^2 \mathbf{g}_k \mathbf{g}_k^*)^{\frac{1}{\nu}} \mathbf{g}_j}{||\mathbf{g}_j||^4}\right]^\nu \tag{8}$$

and since $\mathbf{g}_k \mathbf{g}_k^*$ is an idempotent matrix, the expression becomes:

$$A_v(\xi_j) = \frac{1}{2} s_k^2 \left[\frac{\mathbf{g}_j^* \mathbf{g}_k \mathbf{g}_k^* \mathbf{g}_j}{||\mathbf{g}_j||^4}\right]^\nu = \frac{1}{2} s_k^2 \left[\frac{(\mathbf{g}_j^* \mathbf{g}_k)^2}{||\mathbf{g}_j||^4}\right]^\nu \tag{9}$$

From Eq. (9), it can be seen that the source autopower is written as the source strength multiplied by the point spread function (PSF) powered to the exponent ν. The term in square brackets is equal to 1 when $j = k$, which is when it is considered the real position of the source, while it is lower than 1 when another position is considered. For this reason, the autopower attributed to the sidelobes can be suppressed by choosing an appropriate value for the exponent ν, thus leaving unchanged the real source autopower. This creates the main lobe on the reconstructed image. It is worth mentioning that the dynamic range increases almost linearly with the value ν; thus for an appropriate exponent value, the dynamic range is considerably increased [33]. From a more practical point of view, since the term in square brackets is not perfectly equal to 1 neither for real sources, also the main lobes are sharpened, improving unexpectedly also the array spatial resolution to some extent.

Capon

Capon method was born in signal processing to determine both the signal of interest intensity and the direction of arrival. For the purposes of the present work, the latter application of Capon method is described in the following [35]. Considering the situation in which a signal produced by n sources is detected by an array of m sensors, with $m > n$, the array output $y(t)$ can be modeled as:

$$y(t) = Ax(t) + e(t) \tag{10}$$

where $y(t)$ has dimension m, $x(t)$ is the n-dimensional vector of the source signals, and $e(t)$ represents the noise. In the end, A is an $m\ x\ n$ matrix whose columns are the steering vectors at fixed angle, namely:

$$A = \left(a(\theta_1) a(\theta_2) \ldots a(\theta_n) \right) \tag{11}$$

The angles $\{a(\theta_k)\}$ are DOAs of the present beamforming problem. Without loss of generality, it is possible to make the assumption that $x(t)$ and $e(t)$ are independent Gaussian distributed random variables with zero mean and covariances:

$$E[x(t)x^*(s)] = P\ \delta_{t,s} \tag{12}$$

$$E[e(t)e^*(s)] = \sigma\ I\ \delta_{t,s} \tag{13}$$

By defining $\hat{R}$ as the sample covariance matrix, namely:

$$\hat{R} = \frac{1}{N} \sum_{t=1}^{N} y(t) y^*(t) \tag{14}$$

it is possible to define the DOAs $\{\theta_k\}$ as the n smallest minima of the function:

$$f(\theta) = a^*(\theta) \hat{R}^{-1} a(\theta) \tag{15}$$

Starting from the algorithm just exposed, which is called standard Capon beamforming (SCB), an improved algorithm has been developed and named robust Capon beamforming (RCB) [35]. RCB uses the theoretical basis of SCB with also the assumption that the knowledge of the DOA can be imprecise. In other words, RCB assumes that the only knowledge about a generic steering vector $a(\theta_k)$ is that it belongs to an uncertainty ellipsoid:

$$||a(\theta_k) - \bar{a}||^2 \leq \epsilon \tag{16}$$

where $\bar{a} = a(\theta + \Delta)$, and Δ and ϵ are the parameters which are optimized for the specific problem under investigation. At the end, the difference between SCB and RCB lies in the fact that using RCB instead of SCB, Function (15) is minimized for any steering vector satisfying Eq. (16), with the guarantee of a greater tolerance. In this way, RCB is more "robust" than SCB, with respect to small errors in the DOA identification, and can bring to more reliable results, as discussed in the "Capon" section.

CLEAN-SC

CLEAN-SC is a deconvolution method that starts with an acoustic image obtained by means of conventional beamforming, followed by an iterative phase where the algorithm removes the fake sources that should produce a "cleaned" map [36]. The starting point for conventional beamforming with microphone arrays is the cross-spectral matrix (CSM), which is assumed to be equal to the sum of the incoherent sources

$$\mathbf{C} = \sum_{k=1}^{K} \mathbf{p}_k \mathbf{p}_k^* \tag{17}$$

$\mathbf{p}_k$ are N-dimensional vectors, where $k = 1, 2 \ldots K$, K is the number of sources, and N is the number of microphones. They represent the Fourier transforms of the signals at a frequency f. Equation (17) is valid under the assumption of no-decorrelation of signals from the same source between different microphones and no-additional incoherent noise. Conventional beamforming uses steering vectors, which contain the response of the microphone array to the source signals. For a single source in position $\vec{\xi}$, the component n of the steering vector $\mathbf{g}$, relative to the n-th microphone, reads:

$$g_n(\vec{\xi}) = -\frac{1}{4\pi ||\vec{x}_n - \vec{\xi}||} \exp\left(\frac{-2\pi i f ||\vec{x}_n - \vec{\xi}||}{c} \right) \tag{18}$$

where f is the frequency, c is the sound speed, $\vec{x}_n$ is the position of the n-th microphone, and $\vec{\xi}$ is the source location. Ideally, the steering vectors $\mathbf{g}_k$ are proportional to the source vectors $\mathbf{p}_k = a_k \mathbf{g}_k$, where a_k are the sources complex amplitudes. The CSM of Eq. (17) can be decomposed as:

$$\mathbf{C} = \sum_{k=1}^{K} A_k \mathbf{g}_k \mathbf{g}_k^* \tag{19}$$

in order to detect the location of the sources and to determine associated source powers.

For the sake of simplicity, the simplest case with only one source will be shown. In this case, there is only one vector $\mathbf{g}$ and its source power A can be obtained minimizing the expression:

$$F = \sum_{(m,n)\in S} |(C_{mn} - A g_m g_n^*)|^2 \tag{20}$$

where C_{mn} is the measured CSM and S is a subset of all possible (m-n) combinations with $m \neq n$. The solution is:

$$A = \frac{\sum_{(m,n)\in S} g_m^* C_{mn} g_n}{\sum_{(m,n)\in S} |g_m|^2 |g_n|^2} \tag{21}$$

Defining the CSM C and the normalized steering vectors $\mathbf{w}$ as

$$\bar{C}_{m,n} = \begin{cases} C_{m,n} \text{ for } m \neq n \\ 0 \text{ for } m = n \end{cases} \quad \text{and} \quad \mathbf{w} = \frac{\mathbf{g}}{\left[\sum_{(m,n)\in S} |g_m|^2 |g_n|^2\right]^{1/2}} \tag{22}$$

the source power A of Eq. (21) can be written as:

$$A = \mathbf{w}^* \bar{\mathbf{C}} \mathbf{w} \tag{23}$$

So far, the vector $\mathbf{g}$ and the matrix $\bar{\mathbf{C}}$ have been written without subscripts, because in the assumption of singular source, there is no possibility of misinterpretation. The subscripts have been used only for the element of the vector $\mathbf{g}$, i.e., g_m, which is relative to the m microphone. In the following, the subscripts start to be written as they are essential for the purposes of the algorithm. The reason is that the location of the source must be distinguished from every other location where a secondary fictitious source may take place. If the source is located in position $\vec{\xi}_j$, the relative CSM is equal to:

$$\mathbf{C}_j = \mathbf{g}_j \mathbf{g}_j^* \tag{24}$$

The source power associated with the position $\vec{\xi}_k$, however due to the source present in position $\vec{\xi}_j$, is the PSF and is defined as:

$$A_{jk} = \mathbf{w}_k^* \bar{C}_j \mathbf{w}_k = \mathbf{w}_k^* [\mathbf{g}_j \bar{\mathbf{g}}_j^*] \mathbf{w}_k \tag{25}$$

It follows that $A_{jk} = 1$ when $j = k$, by definition, while A_{jk} should be equal to zero in the other cases, even if this is not true if the number of microphones is finite. The crucial point of the algorithm is that using the PSF is possible to identify the fictitious sources "seen" by the microphones in position different from the source's one. The image can then be cleaned by eliminating them.

- Obtain a source plot by means of conventional beamforming.
- Search the peak location in the dirty map.
- Subtract the appropriately scaled PSF of the peak location from the dirty map.
- Replace this PSF by a clean beam in the peak position.
- Repeat the previous steps until a stop condition is satisfied.

In order to perform the iterative process just described, a so-called "degraded CSM" is defined:

$$\mathbf{D}^{(i)} \quad \text{where} \quad \mathbf{D}^{(0)} = \mathbf{C} \tag{26}$$

and i is the step of the process. The first step produces a dirty map:

$$P_j^{(0)} = \mathbf{w}_j^* \bar{\mathbf{D}}^{(0)} \mathbf{w}_j = \mathbf{w}_j^* \bar{\mathbf{C}} \mathbf{w}_j \tag{27}$$

Writing more explicitly the steps just mentioned:

1. For every location j, a dirty map $P_j^{(i)}$ is produced.
2. The peak location $\vec{\xi}_{max}^{(i)}$ is found looking for the maximum value in $P_j^{(i)}$.
3. The map is updated:

$$P_j^{(i+1)} = P_j^{(i)} - P_{max}^{(i)} \mathbf{w}_j^* [\mathbf{g}_{max}^{(i)} \bar{\mathbf{g}}_{max}^{(i)*}] \mathbf{w}_j \tag{28}$$

4. The PSF is replaced by a clean beam:

$$Q_j^{(i)} = P_{max}^{(i)} \Phi(\vec{\xi}_j - \vec{\xi}_{max}) \tag{29}$$

where the maximum value of the function Φ is $\Phi(0) = 1$.

5. The process is iterated until a stop condition is reached. An example is:

$$||\bar{D}^{(I+1)}|| \geq ||\bar{D}^{(I)}|| \tag{30}$$

The meaning of Eq. (30) is that the process stops when there is more information in the map of a given step than in the map of the previous one, i.e., there are not other useless information to be eliminated, such as sidelobes and reflections.

After I steps, the cleaned map is equal to:

$$A_j = \sum_{i=0}^{I-1} Q_j^{(i)} + P_j^{(I)} \tag{31}$$

and it is expected to contain only real sources.

DAMAS

The Deconvolution Approach for the Mapping of Acoustic Sources (DAMAS) is used to correct array results obtained with conventional beamforming. It consists in the iterative resolution of a unique linear system of equations in order to properly quantify position and strength of acoustic sources [37]. This method starts from the cross-spectral matrix:

$$G_{mm'}(f) = \frac{2}{KTW_s} \sum_{k=1}^{K} \left[P_{mk}^*(f,T) P_{m'k}(f,T)\right] \tag{32}$$

where P_{mk}^* and $P_{m'k}$ are the fast Fourier transforms of the original pressure time records $p_m(t)$ and $p_{m'}(t)$. In Eq. (32), the indices m and m' identify the microphones, which are altogether M, while the index k identifies the sources, which are altogether K. The total record length is $T_{tot} = KT$ and W_s is a data-window weighting constant. An imaginary plane of grid points is placed over the source region, and every point is associated with an M-dimensional steering vector $\mathbf{e}$:

$$\mathbf{e} = [e_1, e_2, \ldots e_M]^T \tag{33}$$

whose elements refer to the M microphones and are equal to:

$$e_m = a_m \frac{r_m}{r_c} \exp\{j2\pi f \tau_m\} \tag{34}$$

For conventional beamforming, the power spectrum obtained from the array is:

$$Y(\mathbf{e}) = \frac{\mathbf{e}^T \mathbf{G} \mathbf{e}}{M^2} \tag{35}$$

where Y is a mean-pressure-squared per frequency bandwidth quantity and the division by the number of microphones serves to standardize the measures to that of an equivalent single microphone one. The analysis of the CSM by means of conventional beamforming brings to the creation of source maps partly due to the effective sources and partly due to the array features. The first step is to link the transform of the pressure measured by the microphone m to a single modeled source located at position n in the source field:

$$P_{mn} = Q_n e_{mn}^{-1} \tag{36}$$

Q_n represents the signal that the microphone m would have measured if flow convection and shear layer refraction had not affected the transmission. Therefore, the product of the pressure transforms present in Eq. (32) can be written as:

$$P_{mn}^* P_{m'n} = (Q_n\, e_{mn}^{-1})^* (Q_n\, e_{m'n}^{-1}) = Q_n^* Q_n (e_{mn}^{-1})^* e_{m'n}^{-1} \tag{37}$$

Then, the modeled microphone array CSM for a single source located in position n can be written as:

$$G_{mod_{mm'}}^n = X_n (e_{mn}^{-1})^* e_{m'n}^{-1} \equiv X_n\, E_{mm'}^n \tag{38}$$

It is now assumed the existence of N statistically independent sources, each at different position n. The total CSM becomes:

$$\mathbf{G}_{mod} = \sum_{n=1}^{N} \mathbf{G}_{mod}^n \tag{39}$$

Inserting this form of the CSM into the expression of the microphone response leads to:

$$Y_{mod}^n = \frac{\mathbf{e}_n^T \mathbf{G}_{mod} \mathbf{e}_n}{M^2} = \frac{\mathbf{e}_n^T \sum_{n'} X_{n'} \mathbf{E}_{n'} \mathbf{e}_n}{M^2} = \sum_{n'} \frac{\mathbf{e}_n^T \mathbf{E}_{n'} \mathbf{e}_n}{M^2} X_{n'} \equiv [\mathbf{AX}]_n \tag{40}$$

therefore, for every position n, the compact notation is obtained:

$$\mathbf{Y} = \mathbf{AX} \tag{41}$$

Equation (41) relates a set of array responses Y_n, relative to spatial positions n, to equivalent source distributions X_n at the same locations. Studying Eq. (41) for acoustic problems of interest, it has been found that the number of linearly independent equations is little compared to the total number of equations, meaning that there is a big number of solutions. The equation that has to be solved is:

$$Y_n = A_{n1}X_1 + A_{n2}X_2 + \ldots + A_{nn}X_n + \ldots + A_{nN}X_N \tag{42}$$

and the goal is to determine all the X_n. Indeed, a noise map can be created by finding the values X_n and assigning to every point the correct intensity of sound generated at that location. The DAMAS algorithm solves Eq. (42) in an iterative way:

$$X_n^{(i)} = Y_n - \left[\sum_{n'=1}^{n-1} A_{nn'} X_{n'}^{(i)} + \sum_{n'=n+1}^{N} A_{nn'} X_{n'}^{(i-1)}\right] \tag{43}$$

using for the first iteration the condition $X_n^{(0)} = 0$ or $X_n^{(0)} = Y_n$. Practical examples show that starting from a totally or partly wrong map, after a proper number of iterations, the correct map can be found by DAMAS algorithm [37].

MUSIC

MUSIC (Multiple Signal Classification), described in Gupta and Kar [38], is a widely used signal analysis technique,

which works on the principle of decomposition of eigenvalues. This method is based on the covariance matrix of the signals and it can be used both for uniform and non-uniform linear arrays. In this mathematical model, it is assumed the existence of K narrow band source signals with the same central frequency f_k. The signals are captured by an array of M microphones, with $M >> K$. The simplest version of the algorithm applies to a linear microphone array whose consecutive elements are equally spaced. The far-field approximation is considered, in the way that every signal can be interpreted as a plane wave that is incident on the array with azimuth angle θ_k, where k lies between 1 and K. The distance d between two consecutive microphones must be less than or equal to the smaller wavelength to be measured. The overlap of all the K signals captured at the time t by the m-th microphone can be written as:

$$x_m(t) = \sum_{k=1}^{K} s_k(t)\, e^{-j(m-1)\frac{2\pi d \sin\theta_k}{\lambda}} + n_m(t) \tag{44}$$

where $n(t)$ is the background noise. If the response function $a_m(\theta_k)$ of array element m to signal source k is defined in the following way:

$$a_m(\theta_k) = e^{-j(m-1)\frac{2\pi d \sin\theta_k}{\lambda}} \tag{45}$$

The response of a generic microphone can be written as:

$$x_m(t) = \sum_{k=1}^{K} a_m(\theta_k) s_k(t) + n_m(t) \tag{46}$$

or in matrix form:

$$X = AS + N \tag{47}$$

where X and N are two M-dimensional vectors, A is a $M \times K$ matrix, and S is a K-dimensional vector, i.e.:

$$X = [x_1(t), x_2(t) ... x_M(t)]^T \tag{48}$$

$$A = [a(\theta_1), a(\theta_2) ... a(\theta_K)] \tag{49}$$

$$a(\theta_k) = [1, e^{-j\phi_k} ... e^{-j(M-1)\phi_k}]^T \text{ where } \quad \phi_k = \frac{2\pi d}{\lambda} \sin\theta_k \tag{50}$$

$$S = [S_1(t), S_2(t) ... S_K(t)]^T \tag{51}$$

$$N = [n_1(t), n_2(t) ... n_M(t)]^T \, . \tag{52}$$

The signals can be decoupled from background noise by using the covariance matrix in the following way:

$$R_X = E[XX^H] = \tag{53}$$

$$= E[(AS + N)(AS + N)^H] = AE[SS^H]A^H + E[NN^H] = \tag{54}$$

$$= AR_S A^H + R_N = AR_S A^H + \sigma^2 I \, , \tag{55}$$

since:

$$A\, E[SN^H] = E[NS^H]\, A = 0 \, . \tag{56}$$

At this point, the algorithm plans to identify the K biggest eigenvalues of the covariance matrix R_X and to attribute them to the M signals, while the remaining $M - K$ eigenvalues represent the background noise. The eigenvalue equation of the covariance matrix R_X for the eigenvalues relative to the background noise reads:

$$R_X v_i = \sigma^2 v_i \text{ , where} i = K+1, K+2 ... M \tag{57}$$

By using Eq. (53):

$$(AR_S A^H + \sigma^2 I) v_i = \sigma^2 v_i \rightarrow AR_S A^H v_i = 0 \tag{58}$$

Then, multiplying both sides by $R_s^{-1}(A^H A)^{-1} A^H$:

$$R_s^{-1}(A^H A)^{-1} A^H A R_S A^H v_i = 0 \rightarrow A^H v_i = 0 \tag{59}$$

Equation (59) means that the eigenvectors relative to the background noise are orthogonal to the columns of the matrix A. However, these columns refer to the K directions of arrival of the source signals. In this way, the correct angle of arrival θ_i can be identified minimizing the expression:

$$P(\theta) = \frac{1}{a^H(\theta) E_n E_n^H a(\theta)} \tag{60}$$

where:

$$E_n = [v_{K+1}, v_{K+2} ... V_M] \tag{61}$$

At this point, looking at Eq. (17), a comparison between CLEAN-SC and MUSIC can be argued. About that, it has been already noticed that Eq. (17), for CLEAN-SC algorithm, is valid under the assumption of no-decorrelation of signals from the same source between different microphones and no-additional incoherent noise. While the former assumption is valid also for the MUSIC algorithm, the latter represent a difference between the two methods. Indeed, as it has just been shown, the MUSIC algorithm takes into account the presence of incoherent noise and exploits it for the identification of the source position.

SONAH

Since its conception, around 1950 in the particle physics field, the technique of the holography has shown its power also in the acoustic field. "Near-field Acoustic Holography" (NAH) is a first application of this method, and its purpose is the visualization of

sound radiation and the localization of noise sources. Good results can be obtained if the measurements are performed over an area which fully covers the positions with higher sound pressure, but this can be hardly satisfied in some cases. A solution to this problem comes from the "Statistically Optimized Near-field Acoustic Holography" (SONAH) [39], which requires that the measured pressure can be represented by a linear combination of plane waves. In order to fully understand SONAH, a mention to "Least-Squared Elementary Wave Model" (LS-EWM) is important as it explicitly computes the coefficients of the linear combination abovementioned, while SONAH computes them implicitly.

The starting point in LS-EWM is the assumption that sound pressure has been measured on a set of I positions in a source-free region Ω. The goal is to reconstruct the sound field in Ω starting from these measured pressures. Using a set of wave functions Ψ_n, the following equation is considered:

$$p(r_i) = \sum_{n=1}^{N} a_n \Psi_n(r_i) \quad \textbf{where} \quad i = 1, 2...I \tag{62}$$

$p(r_i)$ are the measured pressures and a_n are unknown complex expansion coefficients. If $I \geq N$, where N is the dimension of the subspace which is supposed to be generated by the set of wave functions Ψ_n, the equations are more than the unknown coefficients, and the system can be solved finding the least-squares solutions. In a matrix formulation Eq. (62):

$$\mathbf{p} = \mathbf{Ba} \tag{63}$$

where $\mathbf{p}$ is the I-dimensional pressure vector, $\mathbf{B} = \Psi_n(r_i)$ is a IxN wave function matrix, and $\mathbf{a}$ is a N-dimensional vector containing the complex expansion coefficients. With $I \geq N$, the least-squares solution of Eq. (63) is $\mathbf{a} = (\mathbf{B}^H B)^{-1}\mathbf{B}^H\mathbf{p}$. However, the problem is over-determined and a regularization is needed. Using Tikhonov regularization [ref], the solution becomes:

$$\tilde{a} = (\mathbf{B}^H B + \epsilon\mathbf{I})^{-1}\mathbf{B}^H\mathbf{p} \tag{64}$$

Assuming that the set of wave functions Ψ_n constitutes a complete basis in Ω, the sound pressure field can be represented in every point using the functions $\tilde{a}_n$. The reconstructed pressure turns out to be equal to:

$$\tilde{p}(r) = \sum_{n=1}^{N} \tilde{a}_n \Psi_n(r) = \tilde{\mathbf{a}}^T \alpha(r) \tag{65}$$

The LS-EWM computes the reconstructed pressure directly computing the coefficients $a(r_i)$, while SONAH simply requires the reconstructed pressure to be proportional to the measured one. More in details:

$$\tilde{\mathbf{p}}(r) = \mathbf{p}^T \mathbf{c}(r)\ . \tag{66}$$

Using Eq. (65) in Eq. (66), the coefficients $\mathbf{c}(r)$ must satisfy the equation:

$$\mathbf{B}^T \mathbf{c}(r) = \alpha(r) \tag{67}$$

solved by:

$$\mathbf{c}(r) = (\mathbf{A}^H\mathbf{A} + \epsilon\mathbf{I})^{-1}\mathbf{A}^H\alpha(r) \tag{68}$$

where the matrix $\mathbf{A}$ is the transpose of matrix $\mathbf{B}$.

A major difference between LS-EWM and SONAH methods is that the former finds explicitly the coefficients of the wave function linear combination from the measured pressures, and then asks itself how to predict the reconstructed pressure in every point. The latter starts with the prediction problem and then uses the wave function formalism without computing explicitly the coefficients of their linear combination.

On-Field Applications

In the very last years beamforming has been widely applied in acoustics, producing a strong increase of the publications on this subject. As a proof, the search string used on *Scopus* is reported in Table 1. This string provided 175 papers reporting beamforming applications published from 2019 onwards. This growing trend is more evident in the histogram reported in Fig. 1, which shows the time course of the number of publications about beamforming for all the algorithms analyzed in this review. Figure 2 reports an insight for only DAS and FB, as they represent the algorithms with the most significant growth. This increase of publications testifies a continuous increase of interest in the subject and prospects future developments and improvements.

The present chapter provides a synthetic description of the different applications of beamforming for source recognition found in literature, following the algorithm distinction used in the previous section. It is important to clarify that the algorithms investigated in many examples reported are only a part of a more complex procedure. In those cases, the present document does not provide an exhaustive explanation of each tool used, as it would

Table 1 Search string used on *Scopus* to obtain 175 papers reporting beamforming applications published from 2019 onwards

KEY	beamforming AND algorithms AND acoustic
AND NOT KEY	photoacoustic
AND NOT KEY	wireless
AND NOT KEY	ultrasound
AND PUBYEAR	> 2018

diverge from the focus of the performance analysis of algorithms presented in the "Mathematical Formulations of Beamforming Algorithms" section. The review has been carried out on *Scopus*, *PubMed*, and *Web of Science* using the strings reported in Tables 2 and 3. In the following subsections, both new articles published from 2019 onwards and older ones are mentioned. The former are mentioned in order to cite new works which have been carried out after the aforementioned reviews [29•, 30•, 31•]; the latter, even if outdated, are mentioned if they contain essential information that can be useful to draw an effective state-of-the-art. As can be seen from Tables 2 and 3, no applications of SONAH have been found in literature.

The accuracy of an acoustic beamforming measurement and the environmental scenario is estimated analyzing some specific features. The accuracy features used are dynamic range and spatial resolution, while signal-to-noise ratio (SNR) is used as an environmental feature. Dynamic range is the difference between the peak level and the highest sidelobe level of a beam pattern [40]. A high value of the dynamic range means that sources are clearly recognized from reflections. Spatial resolution can be encountered in literature with two meanings, which may seem different but are correlated. The first is the width of the main lobe 3 dB below its peak [40], and the second is the minimum angular resolution at which it is possible to distinguish two different sources which are close one another [30•]. A high value of the spatial resolution means that sources are well located in space. The SNR, instead, is the fraction between the sound emitted by the source under investigation and the background noise. Straightforwardly, it is a measure of how much confusing the scenario is.

Delay and Sum

Different applications of DAS can be found in literature, also in specific tasks such as recognition of noise emitted by chain saws in order to recognize illegal deforestation [41], localization of gunshots [42], or discrimination of cough sounds in the presence of white noise [43]. Other interesting results have been found in the application of DAS to speech recognition, where quite high SNR gains were reached [44], which means a bigger dynamic range and a better estimation of the source level. More in detail, the paper [44] shows that DAS algorithm can give reliable results if the experimental setup of the microphone array is optimized, i.e., a higher

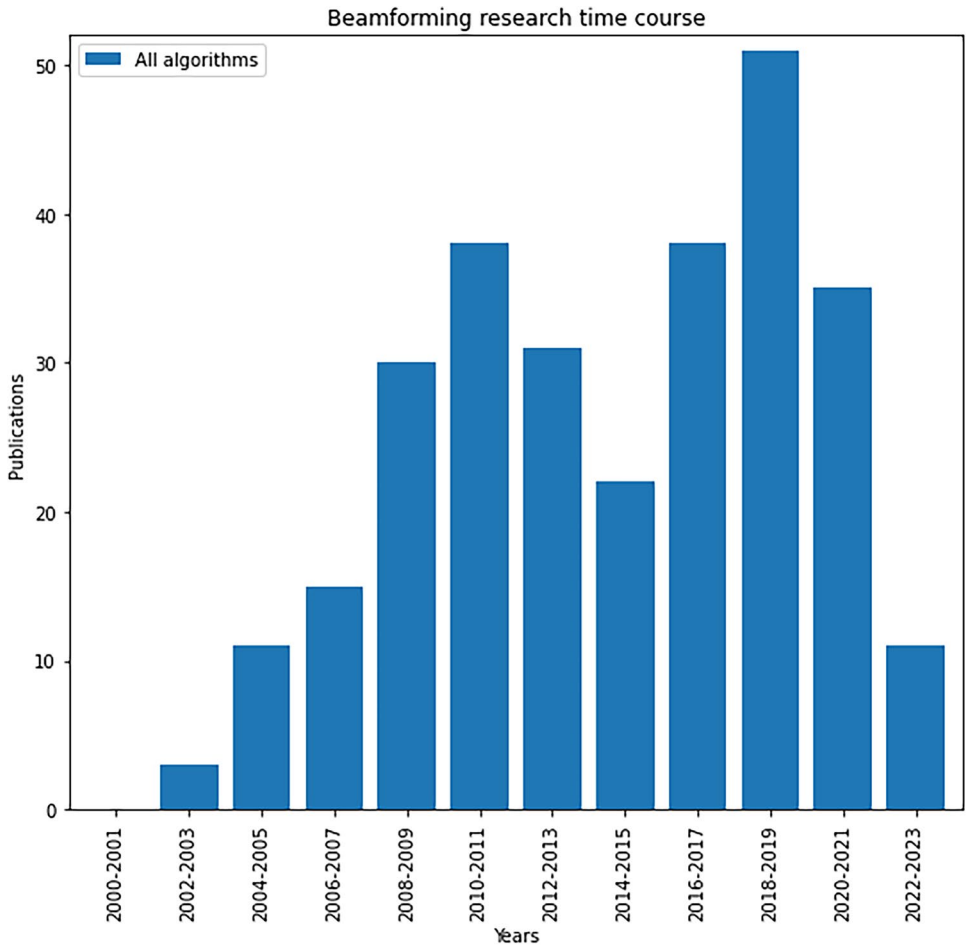

Fig. 1 Histograms of the publications about applications of the algorithms DAS, FB, Capon, MUSIC, EVOB, CLEAN-SC, DAMAS, and SONAH per couple of years

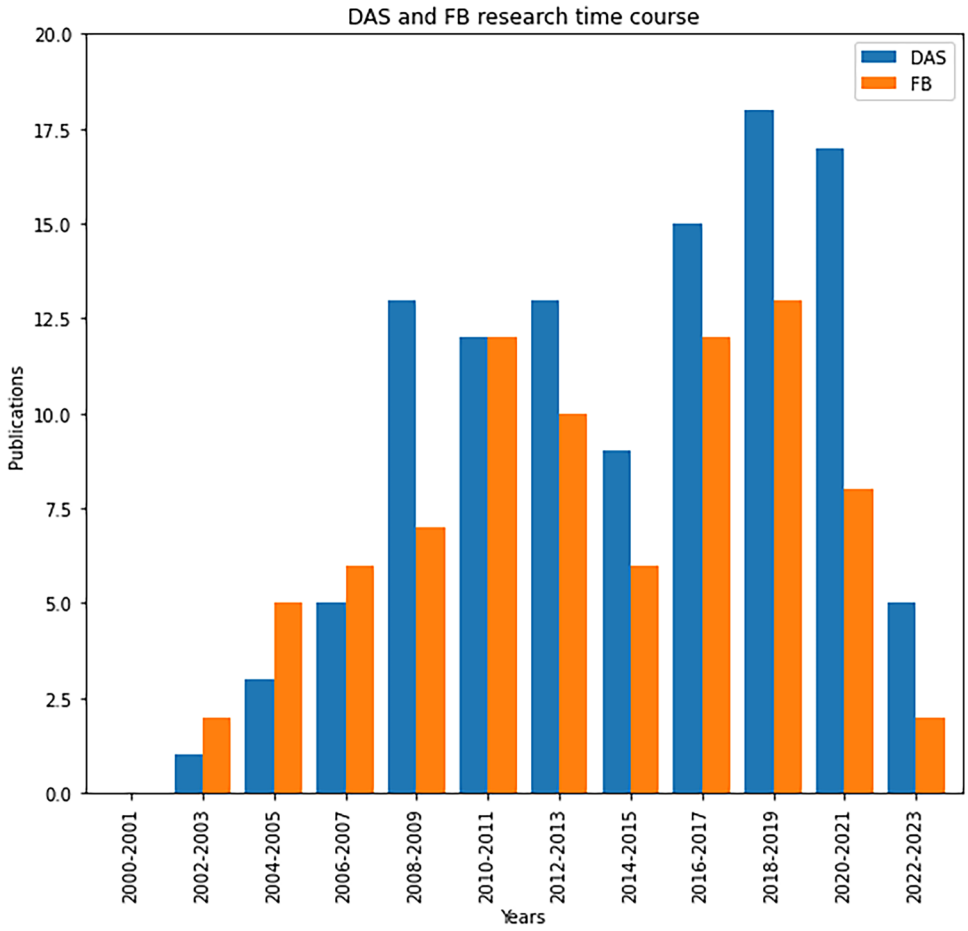

Fig. 2 Histograms of the publications about applications of the algorithms DAS and FB per couple of years

SNR gain can be obtained enlarging the space between the microphones in the array. The reason behind is that speech is mainly made of low frequencies, and then, a larger space between microphones can bring to a more accurate match between the sound wavelength and the lattice size (i.e., distance between two adjacent microphones). Thanks to good results like these, DAS is often regarded as a landmark which shows minimal requirements that a beamforming algorithm must show in order to be acceptable. For this reason, the results of new techniques are often compared to DAS outcomes in the same situation, in order to judge the reliability of the new techniques. Examples of this comparison can be found in Wajid et al. and Gur [45, 46]. Moreover, DAS is also used as a preliminary step before the application of a more complex algorithm, such as CLEAN-SC, as reported in Koop and Ehrenfried [47]. Although these quite good

Table 2 Keywords used for the research in *Scopus* and *PubMed*, together with the number of outcomes. *Only for the algorithm Capon, the string used in *PubMed* was different from that used in *Scopus*, namely in the former, the field "NOT ultrasound" was useless, and for this reason, it was omitted. On the contrary, in *Scopus*, that field was useful in order to avoid misleading results

Algorithm	Research keywords	Scopus	PubMed
DAS	acoustic AND beamforming AND algorithm AND delay and sum AND NOT photoacoustic AND NOT biomedical	58	35
FB	acoustic AND beamforming AND algorithm AND functional	6	70
Capon	acoustic AND beamforming AND algorithm AND capon AND NOT ultrasound	19	7*
CLEAN	acoustic AND beamforming AND algorithm AND clean	4	7
DAMAS	acoustic AND beamforming AND algorithm AND damas	4	5
MUSIC	acoustic AND beamforming AND algorithm AND music	18	3
SONAH	acoustic AND beamforming AND algorithm AND sonah	0	0

Table 3 Keywords used for the research in *Web of Science*, together with the number of outcomes

Algorithm	Research keywords	Web of Science
DAS	acoustic AND beamforming AND delay and sum	16
FB	acoustic AND functional AND beamforming	2
Capon	acoustic AND beamforming AND capon	4
CLEAN	acoustic AND beamforming AND clean	2
DAMAS	acoustic AND beamforming AND damas	4
MUSIC	acoustic AND beamforming AND music	2
SONAH	acoustic AND beamforming AND sonah	0

results, it is well known that in some scenarios, DAS algorithm shows serious shortcomings, such as poor spatial resolution and high sidelobe levels. These lacks are evident when the output of the DAS algorithm is compared to the output of other methods, such as DAMAS. As shown in Ocker and Pannert [48], a virtually rotating array was implemented and the results of simulations and measurements clearly underlined the poor dynamic range and spatial resolution of the DAS algorithm against the high accuracy of the deconvolution method DAMAS. Other comparisons were made with "frequency-difference beamforming" [49], "spherical harmonics beamforming (SHB)" [50], and "circular harmonics beamforming" [51], leading to the observation of an intensification of the poor performances at low frequencies. In order to overcome these issues, some improvements of DAS were attempted making use of a combination of DAS algorithm with other techniques. A first example combines DAS with the "rotational beamforming method" (RBM), which was applied to rotating fan [52]. Results show that this hybrid method can localize better the sound sources and be capable of following their motion. As already stated, one of the main problems of DAS is the presence of high sidelobe levels. In indoor acoustic sound source localization, the most popular algorithm is SHB; nevertheless, in Yang et al. [53], a combined algorithm consisting of functional beamforming (FB) and DAS is claimed to deal with this issue with good results. DAS performed well both on coherent and incoherent sources, but it was also reported by the authors that the presence of sidelobes can be reduced using FB + DAS. A reliable version of the last algorithm for coherent sources is not available. It is worth noting that whereas the results of DAS are independent of the focus distance, the results of FB + DAS showed a problem linked to the growth of the functional parameter when focus distance is different from target-antenna distance or focus direction do not embrace source direction. Another issue which afflicts DAS is the incapability of dealing with noisy background. In Li et al. [54], this problem was solved by applying the "blind source separation" (BSS) as a preliminary step before the application of DAS, with proven ability to distinguish noise sources from background noise. The BSS technique is used to distinguish the different signals which are present in a mixed signal. In this way, after distinguishing the different signals, the one that is under investigation can be localized in space. The problem of high sidelobe levels afflicts DAS in many different situations, for instance when it deals with the task of speech recognition in reverberant environments. An interesting attempt that aims to reduce reflections was presented in Talmon et al. [55], where "Transfer Function Generalized Sidelobe Canceler" (TF-GSC) was combined with DAS. Results showed that the combination TF-GSC + DAS performed better than the TF-GSC alone. A different method used to improve the performance of DAS focuses on the theoretical working of a beamforming algorithm, that is, the covariance matrix. Indeed, since acoustic scenarios showed low SNR, working on the covariance matrix can be useful to reduce the noise and enhance the signal. In Xia et al. [56], the authors fixed the issue by dividing the noise field into symmetrical and asymmetrical noise, and they found that the symmetrical part can only affect the real part of the covariance matrix. Then, the authors separated the covariance matrix into the real and the imaginary parts in order to apply DAS only to the imaginary one. SNR resulted to be improved with the disadvantage that fake source appeared, which are impossible to distinguish from real ones. The solution is not to eliminate completely the real part of the covariance matrix, but instead to reconstruct it using a constrained optimization problem. The authors solved the problem using the particle swarm algorithm [56] to remove false targets. Experimental results showed that the estimation of two sources was improved of about 3 dB using only the imaginary part, and of about 7 dB using also the reconstructed real part. An important field of application of beamforming algorithms is real-time monitoring, as shown in Salom et al. [57], where DAS was implemented on a field-programmable gate array. The accuracy and the computation speed of the algorithm are especially vital here. The former attribute is necessary for the reliability of the system, especially when they are used for health and safety purposes, while the latter is necessary for real-time applications with high-speed performance requirements. An example in this field of application is represented by Bai and Huang [58],

where starting from the assumption that DAS is influenced by background, algorithm such as arithmetic averaging (AA) can be applied to remove the background noise. Anyway, the application of this optimization shows two main problems, that is:

1. Coherent source noise is still present.
2. Real-time capabilities are not available.

Both problems are solved with the introduction of an observer-based approach verified by means of numerical simulations. So far, the possible improvements of DAS algorithm have been discussed, but there are many other influences, external to the algorithm, which should not be neglected. The most important one is the composition of the microphone array. An improvement of this structure can bring to an overall improvement of the efficiency, as it is shown in Lashi et al., Lauterbach et al., and Kates [59–61]. After all, in these works, it is shown that the application of DAS algorithm combined to an optimization of the spatial array can bring such good results that the complexity of other algorithms is not justified and it can be excessive. Other optimizations, such as accurate calibration procedure and parameter uncertainty analysis, may also improve DAS spatial resolution [62, 63] and cannot be neglected.

Functional Beamforming

An interesting application of functional beamforming can be found in Yang et al. [53] and Chu et al. [64], where FB conjecture was combined with other algorithms in order to improve the efficiency of source localization. The first combination is the same that has been already mentioned in the "Delay and Sum" section, namely the combination between FB and DAS. It leads to strong attenuation of sidelobes at improved speed, very useful in indoor measurements. However, the process is not defect free, and poor spatial resolution and low quantification accuracy occurred. Ridge detection (RD) and deconvolution approaches, such as DAMAS, were combined with FB to solve the issues. Computer simulations and experiments were carried out in Chu et al. [64] using these combined tools, showing that FDAS + RD + DAMAS have the same excellent spatial resolution of DAMAS, but it is also capable of providing a stronger sidelobe attenuation and it is two hundreds time faster. Furthermore, FDAS + RD + DAMAS inherits the already mentioned advantages of FDAS alone, but in addition, it improves its low quantification accuracy, regardless of the coincidence between focus distance and source-array distance. The other important application of functional beamforming is in aircraft noise measurements [33, 65]. The work [33] aimed at locating the aircraft elements which are the source of the noise analyzing 115 landing aircraft flyover measurements at Amsterdam Airport Schiphol. The authors acquired data with a 32-microphone array, with 1.7 m diameter in a spiral distribution, and they filtered signals in the range 45–11,200 Hz and applied functional beamforming. A proper choice of the exponent, $\nu = 100$, allowed to significantly reduce the sidelobes, achieving a 30 times larger dynamic range and a 6 times better array spatial resolution. The authors evaluated the performance of functional beamforming in their measurements by comparing FB results to others such as CLEAN-PSF and CLEAN-SC. The authors recommend to consider the following propagation effects before applying any beamforming algorithm to aircraft noise measurements:

1. The Doppler effect since the source is in motion [66].
2. The geometrical spreading from the source to the observer, in order to obtain the emitted SPL from the recorder one.
3. The atmospheric absorption of the sound.

In Merino-Martinez et al. [33], conventional beamforming found a very wide lobe pointing approximately to the nose landing gear location but heavily contaminated by sidelobes, as if it were difficult to identify the noise source. The CLEAN-PSF showed similar results with little improvements. The best results were obtained with functional beamforming and CLEAN-SC, both showing no sidelobes. It was also observed that conventional beamforming and CLEAN-PSF show small values of dynamic range, below 10 dB, while functional beamforming and CLEAN-SC reach bigger values of 90 dB and 160 dB, thus getting a clearer image. A larger dynamic range allows to preserve noise sources with lower amplitude than the strongest one, which would otherwise have been confused within sidelobes, and thus, it represents an improvement. Sophisticated methods such as functional beamforming and CLEAN-SC can then obtain much better results than those obtained by conventional beamforming and CLEAN-PSF. However, it is worth mentioning that CLEAN-SC is unable to identify multiple sources emitting at the same frequency.

Capon

As explained in the "Capon" section, a fundamental aspect is that the steering vectors are the key of the theoretical model behind beamforming. However, they can only partially reproduce the reality. In environmental acoustic measurements, this discrepancy can be very large due to extremely confusing scenarios, and keeping a certain value of tolerance in the determination of the used theoretical tools used, namely the steering vectors in the beamforming field, can be very useful. In

beamforming measurements, this can be done ensuring to the steering vectors a certain range of variation. This challenge is addressed by the so-called adaptive beamforming. One of the main algorithm of this branch is the Capon algorithm and the consequent robust Capon beamforming (RCB). In the papers [67, 68], it is shown how the Capon algorithm's adaptability can be exploited to fix a specific problem in a very complex beamforming procedure. Namely, in these works, the DOA estimation was performed by means of the coherent signal-subspace method (CSM), whose core is a mathematical tool called focusing matrix. The estimation of the focusing matrix is strongly affected by two factors: initial direction estimation and focusing frequency choice. An error in the estimation of one of these two factors would significantly worsen the algorithm response. In the aforementioned papers, the robust Capon beamforming was used to choice properly the two factors of interest, and then to properly determine the focusing matrix. It was found that the CSM algorithm optimized with RCB shows lower sidelobes than the CSM algorithm alone, in many frequency ranges. In the papers [67, 68], the RCB algorithm was used in a very complex beamforming procedure and its functioning was not explained in detail. The explicit way in which the steering vectors are adapted by the Capon algorithm can be seen in Bao et al. [69] and Somasundaram and Parsons [70]. In Bao et al. [69], the correct formula for the estimation of the error allowance in the context of machinery condition monitoring was determined. The error allowance is the mismatch between the steering vectors assumed by the model and the actual ones which better fit the problem under examination. It is represented by a small parameter ϵ defined by:

$$||\mathbf{v}_a - \mathbf{v}||^2 \leq \epsilon \ , \tag{69}$$

where $\mathbf{v}_a$ is one of the actual steering vectors, while $\mathbf{v}$ is one of the steering vectors assumed by the model. In Bao et al. [69], it was found that two parameters very important for the correct estimation of the error allowance are the source-array distance and the incident angle. It was also found that the further the distance of the source from the array and the smaller the incident angle, the greater the appropriate range of the error allowance. Therefore, large distance and small angles have to be preferred in order to obtain good response from the algorithm. In this way, the assumed steering vectors may differ from the actual ones for a greater value without affecting the accuracy of the algorithm. In Somasundaram and Parsons [70], the inaccuracy caused by the a priori choice of steering vector was addressed. The correct parameters, namely the array steering vector errors, were found by exploiting ellipsoidal uncertainty sets [35, 71]. RCB performed the best especially in snapshot-deficient scenarios that, instead, are the scenarios with high probability of identifying the wrong DOA due to poor statistics. Another application of RCB can be found in Bao [72] for moving sources. The performances of RCB were compared to the performances of three algorithms, namely Sample Matrix Inversion (SMI) method [73], Recursive Least Squares method with Sliding Window (RLSSW) [72], and Block Constrained Least Mean Square method with Diagonal Loading (BCLMSDL) [73]. Three criteria were used in Bao [72] to analyze the results: coherence between input and algorithm's output, computational complexity, and robustness of the algorithm with respect to the motion of the sources. The analysis showed that RCB performs better than SMI, RLSSW, and BCLMSDL in all the three criteria, making it more reliable and computationally cheaper. In Azimi-Sadjadi et al. [74], the localization of moving sources was also addressed. It was found that Capon resolves very well and tracks multiple closely spaced sources in tight formations. In Camargo et al. [75], the authors aimed to find a good replacement of CB for the analysis at low frequencies, which is where CB performs poorly. For this task, RCB was compared to CLEAN-SC and CB, and it was found that RCB is able to locate the source (spatial resolution) in a more concentrated way than CB. However, the best performance in this task is provided by CLEAN-SC, which is famous for spatial resolution. It performs the best in identifying the single noisy component among many components in a complex equipment. Despite the good results in DOA estimation, the increasing contrast provided by adaptive beamforming algorithms may not be a direct consequence of their adaptability to the context. In fact, the dynamic range alterations, which can be simply a gray-level transformation of the image, was demonstrated in Rindal et al. [76] to correlate with the contrast ratio and the contrast-to-noise ratio, which are both measurements of the image contrast. Then, further studies are needed to establish if the adaptive beamforming is responsible for the improved results.

CLEAN-SC

Since 2017, only few new works concerning applications of CLEAN-SC algorithm have been published in literature, as it can be seen looking at Tables 2 and 3. The result of He et al. [77] is somehow already known in literature [30•], namely that CLEAN-SC performs better than conventional beamforming. The paper [77] analyzes the correlation between vehicles' interior noise and exterior aerodynamic noise, reaching the conclusion that, switching from conventional beamforming to CLEAN-SC, improvements both in the dynamic range and in the spatial resolution can be appreciated. The reference [78], instead, investigates an application of the CLEAN-SC algorithm revealing that a combination of CLEAN-SC algorithm with a spherical microphone array improves the performance of the CLEAN-PSF algorithm. After mentioning the two previous articles

[77, 78], which, respectively, show the performative superiority of CLEAN-SC with respect to conventional beamforming, and the improvements that can be achieved combining CLEAN-SC with other algorithms, it is worth mentioning another way to improve CLEAN-SC performances. Namely, the following articles show how it is possible to get better results from CLEAN-SC working previously on the scanning surface used by the algorithm. The paper [79] shows how to compress the number of focus grid points participating in the deconvolution algorithm loop, according to the sound source recognition threshold set. This choice is based on the output of FB, previously applied to the data. In this work, it is shown that, following this procedure, the computational efficiency of CLEAN-SC can become 3.9 times higher than that of CLEAN-SC. Another work related to this issue is presented in Legg and Bradley [80]. In this paper, a quite tricky question is addressed, concerning an implicit assumption used in beamforming. The assumption is that the components of a distributed source lay on the same plane. For this reason, the scanning plane considered is usually two-dimensional. For sources whose components do not lay on the same plane, which is reasonably a quite common eventuality, this wrong assumption may lead to inaccuracy in the source localization and in the source sound power estimation. In this paper [80], a new technique for the automatic generation of the 3D map of the scanning surface used by beamforming algorithms is presented. It is demonstrated that source position and source sound power estimated by CLEAN-SC using the new proposed 3D scanning surfaces are more accurate than the ones obtained with conventional 2D scanning surfaces.

DAMAS

DAMAS is another deconvolution method that, as described in the "DAMAS" section, localizes the sources solving an inverse problem. This algorithm reaches high levels of accuracy but it is computationally very expensive. Indeed, the optimization attempts focus on the reduction of the calculation time. The first modification attempt [81] consisted of the application of two constraints to the solution of the inverse problem, namely sparsity and non-negativity of the solution. The constrained problem is then solved by means of the Krylov projection. The whole procedure is shortened with the acronym SNNK. Results showed the merits of this methods compared to other approaches, such as conventional beamforming and DAMAS + Nonnegative Least Squares, both in terms of reconstruction accuracy and computational time. The second attempt [82] was based on the application of convex optimization (CO). By means of wind tunnel measurements, the authors demonstrated that their variant is better than the conventional DAMAS in spatial resolution and dynamic range. Finally, the last improvement focuses on a new compression computational grid. The innovation proposed in the works [83] was to compress computational grid based on CBF and FB and then to choose the compression grid with larger compression ratio. Deconvolution methods are typically meant to "clean" a quite confused image obtained by means of conventional beamforming. For this purpose, they eliminate sidelobes and reflections, but for this reason, they are often applied only to indoor measurements. Besides the post-processing algorithms described above, there is another approach called "Noise Source Localization and Optimization of Phased Array Results" (LORE), which is similar to DAMAS but seems to ensure faster performances. LORE was applied to numerical simulation and indoor experiments [84, 85], showing good results in both cases for a wide range of frequencies and source distribution complexity. Besides the computational time reduction, it overcomes other limitations such as the applicability to small regions in space. Furthermore, it was shown that even when LORE looses accuracy in a specific range of frequencies, due to the sensibility of the microphone array used, the maps reconstructed by means of this method are better than the actual ones.

MUSIC

It is a widely shared opinion that the MUSIC algorithm shows very high level of accuracy, compared to other algorithms. For instance, the authors in [86] showed that for a fixed number of sensors, MUSIC gives better results than other algorithms such as minimum variance distortionless response [87] and 2-dimensional fast Fourier transform [88]. Thanks to its accuracy, it is also used to check the reliability of new experimental setup [89] or as a control tool in acoustic test, such as acoustic impedance of some specific material [90]. Furthermore, it is also used as a benchmark in testing new algorithms' performances [91]. Despite this quality, it is worth noting that MUSIC does not perform very well in all acoustic environment. In fact, it shows some problem in cases of low SNR, few samples, and extended sources and not with point-like ones, as reported for example in Liu et al. [92]. MUSIC algorithm shows a better high spatial resolution than other algorithms in acoustic environment which are not chaotic. For this reason, many authors considered to build a multi-algorithm tool composed by a first part with the task of cleaning the image from background noise and a second part applying MUSIC to this pre-processed image and then clean the signals coming from the main sources, returning a clear image with a high spatial resolution. Three recent applications of this combination can be found in literature. In the first [93], the authors used the summation beamforming algorithm (SBA) as a first step to establish a search range and then the MUSIC algorithm in the last step to obtain the final image. The results shown in this work confirm the feasibility and the reliability of this method,

but the main concern addressed by the authors is about the very high demand in computations to feed the MUSIC algorithm with the initial input, because of the complexity of this accurate method. Therefore, the solution was to previously simplify the original data. A second composite algorithm with MUSIC was presented in Fan et al. [94], where the algorithm consisted of three steps: a conventional beamforming was firstly applied to detect targets' location; in the second step, blind source separation (BSS) was used in order to make targets statistically independent from each other. Finally, in the third step, MUSIC was applied to improve the accuracy of the acoustic map obtained from the previous steps. The last experiment compared the results obtained using the MUSIC algorithm with the results obtained using an algorithm which pre-processes the image by means of "independent component analysis" and then applying a modified version of the MUSIC algorithm to locate the sources. The variant of the MUSIC algorithm used is built with the "constrained optimization method." In both these last two cases, some experiments were carried out using only the MUSIC algorithm and others using these composite algorithms, with the latter showing better results. In light of this, it is possible to state that the composite versions are preferable to the MUSIC algorithm alone. The reason is that the MUSIC algorithm shows a high computational complexity and the inability to process image with a very noisy background, and therefore, it performs better if it is fed with pre-processed and simplified signals. Another solution to the abovementioned limitations of MUSIC is to implement some modified version of the algorithm. Two interesting variants of MUSIC were presented in Kassis and Picheral [95] and Xiao et al. [96], which respectively show how zero-forcing MUSIC and W2D-MUSIC perform better than the MUSIC algorithm alone. A detailed description is remanded to the original papers. Even with its difficulties in particular scenario, MUSIC is a very reliable algorithm also used in medical analysis [97] and in preventing health injuries in industrial scenarios [98].

Discussion and Conclusions

The present paper reviewed the recent scientific literature on beamforming algorithms, a topic that had a boom in the very last years. The issue has been addressed from both theoretical and experimental points of view, highlighting advantages and disadvantages of the most used algorithms. The theoretical part reported in the "Mathematical Formulations of Beamforming Algorithms" section aimed at improving the awareness and background knowledge by collecting and presenting in an academical way the mathematical formulation behind the most used beamforming algorithms. The section would be of interest for scientists but also be a detailed guide for acoustic camera users in the difficult choice of what algorithm better fit the particular scenario under investigation. The latter ones can then extend the utility beyond the theoretical analysis by means of the state-of-the-art on the algorithm applications reported in the "On-Field Applications" section, showing how others have used the algorithms in different situations. In Table 4, a summary of the strengths and of the weaknesses of each algorithm is provided. In Table 5, instead, the improvements deriving from the combination of different algorithms are highlighted.

Delay and Sum (DAS) is the conventional beamforming algorithm and, over time, showed poor spatial resolution and high sidelobe levels especially at low frequencies, with a consequent high risk of creating fake sources. However, for research purposes, DAS is still being used in combined procedures with other algorithms in order to improve their performances. In this cases, DAS can be used as a preliminary step and its output is improved by a secondary algorithm such as CLEAN-SC [47]. DAS can also be used as a secondary algorithm after the application of another one in order to obtain better results, as shown in Yang et al. [53] where it is shown how DAS performs better with inputs having better SNR, which are pre-processed by other algorithms in a previous stage. Functional beamforming (FB) is the other conventional beamforming algorithm investigated and, as DAS, it also showed poor spatial resolution. The analysis of FB applications in literature is an example of how theoretical analysis is not sufficient for an exhaustive comprehension of advantages and disadvantages of an algorithm, while field attempts are always useful and fruitful to bring unpredicted results. In fact, the theoretical formulation of FB suggests that its output should show a large sidelobe suppression thanks to the exponent ν of Eq. (9) which suppresses every autopower different from the one related to the actual localization of the source. This should lead to deem sufficient the use of this algorithm and could deter further attempts. However, applications showed that better suppression of sidelobes and dynamic range are ensured when FB is combined with DAS or, even better, with CLEAN-SC algorithm. Furthermore, an improvement of conventional beamforming, namely adaptive beamforming, has been investigated. The analysis showed the adaptability exhibited by this method in complicated scenarios, for instance snapshot-deficient ones. A snapshot-deficient scenario is a situation in which the AC acquired only few images or short videos of the situation, or when the source was active for a short period. Basically, it occurs when few data are available. In these cases, adaptive beamforming can improve spatial resolution and reduce sidelobe levels. Deconvolution algorithms (CLEAN-SC, DAMAS) are known in literature for their good spatial resolution and dynamic range in the outputs. The present paper confirms their reputation, even if some shortcomings emerged: CLEAN-SC have difficulties in the identification of multiple sources emitting at the

Table 4 Summary of weaknesses and strengths of the different algorithms. In order to deepen these types of information, the reader is invited to look at the subsections indicated in the last column

Algorithms	Weaknesses	Strengths	Sections
DAS	Poor spatial resolution and high sidelobe levels	Computationally cheap and easily usable	"Delay and Sum," "Functional Beamforming," "Capon," "CLEAN-SC," "DAMAS," "MUSIC," "Discussion and Conclusions" sections
FB	Poor spatial resolution	Strong theoretical potential	"Functional Beamforming," "Capon," "CLEAN-SC," "DAMAS," "MUSIC," "Discussion and Conclusions" sections
Capon	Further investigation is necessary	Good performances in snapshot-deficient scenarios	"Capon," "CLEAN-SC," "DAMAS," "MUSIC," "Discussion and Conclusions" sections
CLEAN-SC	Difficulties in the identification of multiple sources emitting at the same frequency	High performances in spatial resolution and dynamic range	"CLEAN-SC," "DAMAS," "MUSIC," "Discussion and Conclusions" sections
DAMAS	Computationally expensive	High performances in spatial resolution and dynamic range	"DAMAS," "MUSIC," "Discussion and Conclusions" sections
MUSIC	Problems in scenarios with low SNR, with few samples, and with extended sources	High performances in spatial resolution and dynamic range	"MUSIC," "Discussion and Conclusions" sections

same frequency, while DAMAS is computationally very expensive. Furthermore, also, the CSM eigenvalue decomposition framework has been investigated, with the MUSIC algorithm. MUSIC also shows good spatial resolution and dynamic range, but also presents problems in scenarios with low SNR, when few samples are available or when extended

Table 5 In the left column are reported various combinations of algorithms analyzed in this review. These combinations are claimed to improve the work done by every algorithm alone. In the central column, the relative improvements attested in literature are specified. In the right column, the sections of the present paper in which the reader can find deeper explanations of the cited improvements are indicated

Combinations of algorithms	Improvements	Section
RBM + DAS	Better localization of rotating sources	"Delay and Sum"
FB + DAS	Better results in indoor measurements and sidelobe reduction	"Delay and Sum"
BSS + DAS	Better isolation from background noise	"Delay and Sum"
TF-GSC + DAS	Improvements in speech recognition in reverberant environments	"Delay and Sum"
AA + DAS	Better isolation from background noise	"Delay and Sum"
FDAS + RD + DAMAS	Indoor advantages of FDAS alone + improvements in low quantification accuracy, regardless of the coincidence between focus distance and source-array distance	"Functional Beamforming"
FDAS + RD + DAMAS	Same excellent spatial resolution of DAMAS + better capability to provide stronger sidelobes attenuation + speed improvements	"Functional Beamforming"
CLEAN + compressed focus grid points	Computational efficiency quadrupled	"CLEAN-SC"
CLEAN + automatic generation of 3D source map	More accurate source position and source sound power estimation compared to the ones obtained with conventional 2D scanning surfaces	"CLEAN-SC"
SNNK + DAMAS	Reduction of computational time	"DAMAS"
CO + DAMAS	Better spatial resolution and dynamic range	"DAMAS"
LORE	Faster performances with respect to DAMAS and better applicability to small regions in space	"DAMAS"
SBA + MUSIC	Reduction of computational time with respect to the application of MUSIC alone	"MUSIC"
CB + BSS + MUSIC	Improvements of acoustic map accuracy with respect to the application of CB alone and reduction of computational time with respect to the application of MUSIC alone	"MUSIC"

sources are investigated. In the end, it is also computationally very expensive. The last problem cited led different authors to study different solutions in order to reduce the computational time of these algorithms. Also for deconvolution algorithms, the best solution to solve all these issues remains the use of composed algorithms. All deconvolution algorithms have high spatial resolution, but the correctness of source location has not been actually evaluated in any of the studies found in literature. In this regard, a future work by the authors will investigate it in terms of the distance between the real emission point and the one identified on video by the different algorithms. Finally, the holographic algorithm SONAH has been analyzed, but only from a theoretical point of view, since no recent applications are published in literature. As SONAH is based on a theoretical ground not specifically designed for the environmental acoustics, on-field tests of its reliability are necessary.

One of the aims of the present work was to provide an answer to acoustic camera users on which algorithm is best to use in different scenarios. The literature review has not shown studies that have carried out comparisons between algorithms in the same scenario. The authors highlight the need for such a study and expect that this work will encourage the scientific community in this direction. Even without direct comparisons, but only using the informations found about applications and theoretical approach, it is possible to generally suggest the use of a deconvolution algorithms (CLEAN-SC, DAMAS) or MUSIC, as they showed the best accuracy among algorithms, even if they are slower and more complex. They also have limitations in specific cases, but at present, they represent the best choice for technicians using acoustic cameras with software already implemented. For research purposes, where scientists are dedicated to developing their own algorithms, the best choice currently seems to be the combination of deconvolution algorithms with others. The authors' hope is that this research of combined algorithms will be implemented in the software of acoustic cameras on the market in the future.

Appendix. Basic Concepts of Beamforming

A.1 Introduction

In acoustics, the computation of acoustic pressure in some points of the space, knowing position and strength of the sources, is called direct problem. Beamforming deals with the inverse problem, namely the estimation of position and strength of the sources, starting from measurements taken in some control points of the space. When starting to deal with this kind of problem, an operator could be brought to use a single microphone, as in other kind of acoustic measurements is done. Anyway, a sound measurement performed with a single microphone does not allow the spatial localization of the emitter, as a single microphone can only record the sound pressure field. The response of a microphone, with respect to the arrival angle of the sound, depends on the directivity of the transducer under analysis. The main typologies of directivity are omnidirectional (if the response is equal for every arrival angle of the sound), bidirectional (if 0° and 180° are favored), unidirectional (if only frontal direction is favored), and superdirectional (if the favored direction is frontal with a narrower opening angle with respect to unidirectional one). A single microphone usually shows a very broad polar response. The only exception is represented by superdirectional microphones, used to identify the exact localization of the source. Even though, the great directivity index shown by this typology of microphones is not sufficient to build functional and reliable methods for source localization. The reason is that it would be necessary to look for the maximum response angle and then move the microphone according to this information. It is straightforward to understand that the resulting technique would be slow and inefficient. This awareness brings to the idea of building an array of microphones in order to exploit the delays between microphones and then finding the arrival angle.

Consider the simplest explanation of the problem before moving on to a more articulated treatment. Assuming sources at great distance from the array, the polar angle can be neglected and only the azimuthal one can be considered. This brings to a simplification of the problem into a linear array. Anyway, the implied assumption is that the source is still enough distant from the array to allow to consider the wave front as a plane wave front. The unidimensional treatment of this challenge is showed in Fig. 3.

The plane wave front impacts the different microphones in different times because of the inclination of the wave front with respect to the array. In particular, when the wave front impacts the first microphone, the sound perturbation is still distant from the second microphone for a distance equal to l. Calling α the angle between the wave front and the microphone array, which is the unknown quantity of the problem, and calling d the distance between two consequent microphones of the array, which is known, the distance l is equal to $l = d \sin \alpha$. Furthermore, the distance l is traveled by the wave front in a time equal to $\Delta t = l/c$, where c is the sound speed. Therefore, the delay between the first and the second microphone can be computed, using known quantities, as:

$$\Delta t = \frac{d \sin \alpha}{c} \tag{70}$$

Straightforwardly, the delay between the first microphone and the other ones from the third onwards is a multiple of the time interval computed in Eq. (70). In this way, measuring the delays with which the peak is registered in two

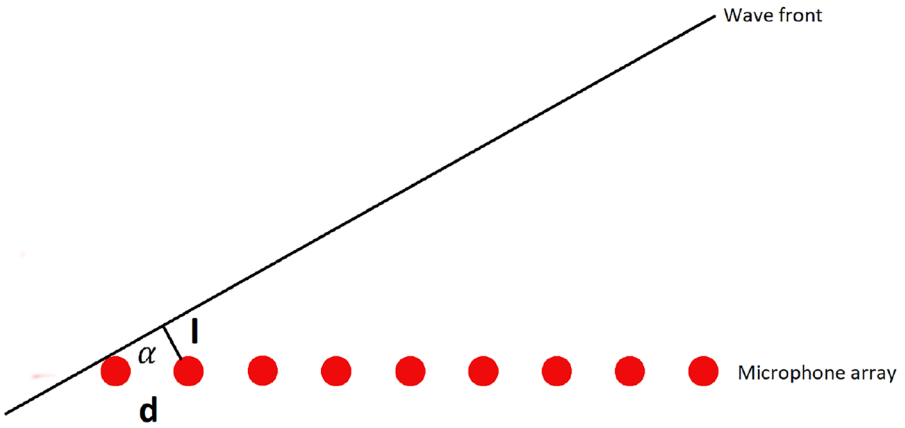

Fig. 3 Scheme of the interaction between a plane wave and a linear microphone array

consequent microphones of the array, which are equal to Δt, is possible to compute the azimuthal arrival angle, using the inverse of Eq. (70)

$$\alpha = \arcsin\left(\frac{c\Delta t}{d}\right) \tag{71}$$

Up to this point, the treatment has been restricted to a single angle and a single frequency problem, just to explain in a simple way the task. For nearest sources, the azimuthal angle is not sufficient and it is necessary to introduce the polar angle, switching to a bidimensional planar array. These few lines aim to introduce the problem and explain why a bidimensional array is required for an optimal resolution of the beamforming task. Another remarkable detail regards the disposition in space of the microphones. Indeed, it is common to see bidimensional microphone arrays with irregular shape. The reason lies in the will to avoid spatial aliasing, that is, a sampling error due to inadequate distance of the microphones for some wavelengths. It is the same effect occurring in the time domain when the sampling frequency is not adequate. It has been found out that severe sampling problems occur when periodic arrays are employed, and that these problems can be solved using arrays with irregular shape [30•].

A.2 Mathematical Formulation of Beamforming

After this brief and simple introduction to the problem, it is now possible to switch to a more advanced treatment of the topic, which introduces the basic concepts of beamforming. An exhaustive treatment of the subject can be found in Allen et al. [32]. Suppose having an array composed by N microphones, so that a generic microphone is identified with the letter n, and a grid of points in the space to be investigated because they can contain the sources. A generic grid point is identified with x_s. As input, beamforming algorithms take sound pressure signals acquired by the array of microphones. Each signal acquired by a microphone is thought as the real signal emitted by a source, modified by the path traveled. To reflect this idea, for each point in the space, the signal acquired by a microphone is modeled as the product between a propagation factor $C_n(x_s)$ and a source function $S(x_s, t)$. The propagation factor is equal to

$$C_n(x_s) = \frac{e^{-i\omega\sigma(x_n, x_s)}}{D(x_n, x_s)} \tag{72}$$

where the numerator accounts for the delay while the denominator for the damping of the signal during the path. The source function $S(x_s, t)$, instead, represents the distribution of sources in space. The basic assumption is that sources associated with different points in space are uncorrelated, namely

$$\langle S^*(x_s', t)S(x_s, t)\rangle = q(x_s)\delta(x_s' - x_s) \tag{73}$$

where $q(x_s)$ is the mean square source strength at x_s and $\langle\rangle$ is the time average defined by

$$\langle f(t)\rangle = \frac{1}{T}\int_0^T f(t)dt\ . \tag{74}$$

For an extended source, the total signal $u_n(t)$ at each microphone is modeled as

$$u_n(t) = \int C_n(x_s)S(x_s, t)d^3x_s + E_n(t) \tag{75}$$

where $E_n(t)$ is the background noise. In the inverse problem framework, the signal $u_n(t)$ acquired by each microphone is the known variable, while source function $S(x_s, t)$ is the unknown variable to be determined. The signal acquired by each microphone is both represented by concrete data and by a theoretical model (75), and the beamforming goal is to estimate the function $S(x_s, t)$ extrapolating it from (75). Collecting all the $u_n(t)$, $C_n(x_s)$, and $E_n(t)$ in vectors of dimension N, $\vec{u}(t)$, $\vec{C}(x_s)$, and $\vec{E}(t)$, it is possible to write Eq. (75) in vectorial notation as

$$\vec{u}(t) = \int \vec{C}(x_s) S(x_s, t) d^3 x_s + \vec{E}(t) \ . \tag{76}$$

At this point, a very important tool is introduced, that is, the set of microphone weight vectors $\vec{w}(x_b)$, defined for every potential source of interest. The task assigned to these vectors is to delay the signal of each microphone of the array, in order to "steer" the array towards the direction which is supposed to be the direction of arrival of the signal. For this reason, they are also called "steering vectors." By definition, they are normalized, i.e.,

$$\vec{w}^{\dagger}(x_b)\vec{w}(x_b) = 1 \ . \tag{77}$$

A "beamforming value" related to the measured signal $\vec{u}(t)$ and the point x_b is computed using the steering vectors. Namely, the scalar product between the signal $\vec{u}(t)$ and the steering vector $\vec{w}(x_b)$ is computed, in order to obtain the "steered" version of $\vec{u}(t)$ towards the direction x_b. From this product, the "beamforming value" of interest is obtained and plotted for every potential point. In mathematical language, this sentence is equal to

$$b(x_b) = \langle |\vec{w}^{\dagger}(x_b)\vec{u}(t)|^2 \rangle \tag{78}$$

Exploiting Eqs. (73) and (77), it is possible to show that, from a theoretical point of view, it is possible to show that for a direction x_b containing an actual source, $b(x_b)$ is equal to the time-average square source strength q, multiplied by the sum of the squares of the propagation factors. Namely

$$b(x_b) = q \ \vec{C}^{\dagger}(x_b)\vec{C}(x_b) = q \sum_{n=1}^{N} |C_n(x_b)|^2 \tag{79}$$

The expression $q \ |C_n(x_b)|^2$ can be thought as the time-average square pressure experienced by a generic microphone n due to the signal produced by the source in x_b, because it is equal to the time-average square source strength q modified by the path traveled until reaching microphone n. Therefore, Eq. (79) shows that, for an actual source in x_b, $b(x_b)$ is equal to the sum over the array of these time-average square pressures due to the presence of the source in x_b. Equation (78) can be expanded, obtaining

$$b(x_b) = \langle |\vec{w}^{\dagger}(x_b)\vec{u}(t)|^2 \rangle = \langle \vec{w}^{\dagger}(x_b)\vec{u}(t)\vec{u}^{\dagger}(t)\vec{w}(x_b) \rangle \tag{80}$$

The product $\langle \vec{u}(t)\vec{u}^{\dagger}(t) \rangle$ is equal to the cross-spectral matrix (CSM). CSM is, in the frequency domain, the analogue of the cross-correlation in the time domain. It can be finally obtained

$$b(x_b) = \vec{w}^{\dagger}(x_b) \ CSM \ \vec{w}(x_b) \tag{81}$$

which is the operative equation of beamforming. The goal of the simplest version of beamforming is to find the set of weight vectors $\vec{w}(x_b)$ which allows to get the maximum value of $b(x_b)$ for a specific direction x_b, because this would mean that in x_b, an actual source is present. In other words, it is necessary to find the set of $\vec{w}(x_b)$ which is able to "steer" the array towards the correct direction. As stated before, the CSM is obtained time-averaging the scalar product between real data collected by microphones and their conjugate transpose. Therefore, the last unknown variables left to compute Eq. (81) are the steering vectors $\vec{w}(x_b)$. Up to this point, an explicit form of $\vec{w}(x_b)$ has not been given. This is the last missing information to complete the theoretical formulation of the problem. Actually, from Eqs. (76) and (77), the choice of the explicit form of the steering vectors is straightforward. Indeed, if, in order to maximize $b(x_b)$, the goal is to maximize the expression

$$\vec{w}^{\dagger}(x_b)\vec{u}(t) = \int \vec{w}^{\dagger}(x_b)\vec{C}(x_s) S(x_s, t) d^3 x_s + \vec{E}(t) \tag{82}$$

it follows that the scalar product $\vec{w}^{\dagger}(x_b)\vec{C}(x_s)$ must be maximized, and this happens when $\vec{w}^{\dagger}(x_b)$ and $\vec{C}(x_s)$ are parallel. Given this constraint and also the constraint shown in Eq. (77), it is straightforward to choose the following form of the steering vectors

$$\vec{w}(x_b) = \frac{\vec{C}(x_b)}{||\vec{C}(x_b)||} \tag{83}$$

Given this expression for the steering vectors, the task of conventional beamforming procedure is to compute the CSM using the data acquired by the microphones and then to find the correct direction x_b wherewith obtaining the maximum value of $b(x_b)$ using Eq. (81). Of course, the most advanced algorithm functioning extends far beyond this simple mathematical formulation and how it is fully shown in the "Mathematical Formulations of Beamforming Algorithms" section. However, it is useful to see this basic treatment of the problem, both because it is the basis of more advanced algorithms and also because it explains the basic idea behind beamforming, from which the current research field originated.

Author Contribution Conceptualization, L.F.; data curation, F.A. and M.B.; formal analysis, F.A., A.M., M.B., L.F.; funding acquisition, F.F. and G.L.; investigation, F.A. and L.F.; methodology, L.F.; project administration, F.F. and G.L.; resources, F.F. and G.L.; supervision, L.F., F.F., and G.L.; validation, L.F.; visualization, G.L.; writing—original draft, F.A., A.M., M.B., and L.F.; writing—review and editing, L.F., F.A., A.M., F.F., and G.L. All authors have read and agreed to the published version of the manuscript.

Funding This work was supported by the funding from the PhD Food and sustainable development—F.A.I. Lab Project (Candidate ID: 10460)—dedicated to the study of the vibro-acoustic impact of agricultural machinery on the environment and on humans.

Compliance with Ethical Standards

Conflict of Interest The authors declare no competing interests.

Human and Animal Rights and Informed Consent This article does not contain any studies with human or animal subjects performed by any of the authors.

References

Papers of particular interest, published recently, have been highlighted as:
- Of importance

1. Billingsley J, Kinns R. The acoustic telescope. 1976;48(4):485–510. https://doi.org/10.1016/0022-460X(76)90552-6.
2. Michel U. History of acoustic beamforming. In: Proceedings of the Berlin Beamforming Conference. 2006. p. 1–17.
3. Acoular. Acoustic testing and source mapping software.http://acoular.org/. (Last accessed date 26/05/2023).
4. Licitra G, Fredianelli L, Kanka S, Artuso F, Fidecaro F. Acoustic comfort in yachts: Measurements with acoustic camera. In: Proceedings of the 28th International Congress on Sound and Vibration. Singapore; 2022. p. 24–8.
5. Kanka S, Fredianelli L, Artuso F, Fidecaro F, Licitra G. Evaluation of acoustic comfort and sound energy transmission in a yacht. Energies. 2023;16(2):808. https://doi.org/10.3390/en16020808.
6. Castellini P, Sassaroli A. Acoustic source localization in a reverberant environment by average beamforming. Mech Syst Signal Process. 2010;24(3):796–808. https://doi.org/10.1016/j.ymssp.2009.10.021.
7. Noh H-M, Choi J-W. Identification of low-frequency noise sources in high-speed train via resolution improvement. J Mech Sci Technol. 2015;29:3609–15. https://doi.org/10.1007/s12206-015-0804-8.
8. Ballesteros JA, Sarradj E, Fernandez MD, Geyer TF, Ballesteros MJ. Noise source identification with beamforming in the pass-by of a car. Appl Acoust. 2015;93:106–19. https://doi.org/10.1016/j.apacoust.2015.01.019.
9. Bourgeois J, Minker W. Time-domain beamforming and blind source separation: Speech input in the car environment, vol. 3. 2009. https://doi.org/10.1007/978-0-387-68836-7.
10. Huanxian B, Huang X, Zhang X. An overview of testing methods for aeroengine fan noise. Prog Aerosp Sci. 2021;124. https://doi.org/10.1016/j.paerosci.2021.100722.
11. Joshi A, Rahman MM, Hickey J-P. Recent advances in passive acoustic localization methods via aircraft and wake vortex aeroacoustics. Fluids. 2022;7(7). https://doi.org/10.3390/fluids7070218.
12. Bu H, Huang X, Zhang X. An overview of testing methods for aeroengine fan noise. Prog Aerosp Sci. 2021;124:100722. https://doi.org/10.1016/j.paerosci.2021.100722.
13. Martin G, Simon F, Biron D. Detection of acoustic radiating areas of a generic helicopter cabin by beamforming. J Acoust Soc Am. 2008;123(5):3310–3310.
14. Sun S, Wang T, Yang H, Chu F. Damage identification of wind turbine blades using an adaptive method for compressive beamforming based on the generalized minimax-concave penalty function. Renew Energy. 2021;181. https://doi.org/10.1016/j.renene.2021.09.024.
15. Wang W, Xue Y, He C, Zhao Y. Review of the typical damage and damage-detection methods of large wind turbine blades. Energies. 2022;15(15). https://doi.org/10.3390/en15155672.
16. Malgoezar A, Vieira A, Snellen M, Simons D, Veldhuis L. Experimental characterization of noise radiation from a ducted propeller of an unmanned aerial vehicle. Int J Aeroacoust. 2019;18:1475472–985295. https://doi.org/10.1177/1475472X19852952.
17. Sahu S, Kumar K, Majumdar A, Kumar AA, Chandra MG. Acoustic-based machine anomaly detection using beamforming and sequential transform learning. 2023;7(2). https://doi.org/10.1109/LSENS.2023.3235049.
18. Benedek T, Tóth P. Beamforming measurements of an axial fan in an industrial environment. 2013;57(2):37–46. https://doi.org/10.3311/PPme.7043.
19. Lanslots J, Deblauwe F, Janssens K. Selecting sound source localization techniques for industrial applications. 2010;44(6):6–10.
20. Amoiridis O, Zarri A, Zamponi R, Pasco Y, Yakhina G, Moreau S, Christophe J, Schram C. Sound localization and quantification analysis of an automotive engine cooling module. J Sound Vib. 2021. https://doi.org/10.1016/j.jsv.2021.116534.
21. Bocanegra JA, Borelli D, Gaggero T, Rizzuto E, Schenone C. A novel approach to port noise characterization using an acoustic camera. Sci Total Environ. 2022;808:151903. https://doi.org/10.1016/j.scitotenv.2021.151903.
22. Fredianelli L, Bernardini M, Tonetti F, Artuso F, Fidecaro F, Licitra G. Acoustic source localization in ports with different beamforming algorithms. In: Proceedings of 51st INTERNOISE Congress. Glasgow; 2022. p. 21–4.
23. Wijnings PWA, Stuijk S, Vries BD, Corporaal H. Robust Bayesian beamforming for sources at different distances with applications in urban monitoring. 2019;4325–9. https://doi.org/10.1109/ICASSP.2019.8682835.
24. Leiba R, Ollivier F, Marchal J, Misdariis N, Marchiano R. Large array of microphones for the automatic recognition of acoustic sources in urban environment, vol. 2017. 2017.
25. Wajid M, Alam F, Yadav S, Khan MA, Usman M. Support vector regression based direction of arrival estimation of an acoustic source. 2020. https://doi.org/10.1109/3ICT51146.2020.9311948.
26. Jin J, Pan N, Chen J, Benesty J, Yang Y. A binaural heterophasic adaptive beamformer and its deep learning assisted implementation. 2023;168:24–30. https://doi.org/10.1016/j.patrec.2023.02.025.
27. Feng L, Zan M, Huang L, Xu Z. A double-step grid-free method for sound source identification using deep learning. 2022;201. https://doi.org/10.1016/j.apacoust.2022.109099.
28. Šarić Z, Subotić M, Bilibajkić R, Barjaktarović M, Stojanović J. Supervised speech separation combined with adaptive beamforming. 2022;76. https://doi.org/10.1016/j.csl.2022.101409.
29. • Leclère Q, Pereira A, Bailly C, Antoni J, Picard C. A unified formalism for acoustic imaging based on microphone array measurements. Int J Aeroacoust. 2017;16:431–56. https://doi.org/10.1177/1475472X17718883. **This reference stands out among other works in literature because it attempts to provide a unified formalism of the different imaging techniques. This harmonization attempt can represent a decisive step forward in the development of this research field**.
30. • Chiariotti P, Martarelli M, Castellini P. Acoustic beamforming for noise source localization - reviews, methodology and applications. Mech Syst Signal Process. 2019;120:422–48. https://doi.org/10.1016/j.ymssp.2018.09.019. **This reference is marked as important because it effectively introduces to the beamforming topic, starting from the basic concepts on to the most advanced algorithms, passing through related topics which are useful to the complete construction of the framework**.
31. • Merino-Martínez R, Sijtsma P, Snellen M, Ahlefeldt T, Antoni J, Bahr CJ, Blacodon D, Ernst D, Finez A, Funke S, Geyer TF,

Haxter S, Herold G, Huang X, Humphreys WM, Leclère Q, Malgoezar A, Michel U, Padois T, Pereira A, Picard C, Sarradj E, Siller HA, Simons DG, Spehr C. A review of acoustic imaging methods using phased microphone arrays. CEAS Aeronaut J. 2019;10:197–230. https://doi.org/10.1007/S13272-019-00383-4. **This review deserves to be emphasized because it attempts to point out the suitability of the different techniques according to the different on-field scenarios. This suggestions are based both on a theoretical and an experimental analyses of the current state-of-the-art**.

32. Allen CS, Blake WK, Dougherty RP, Lynch D, Soderman PT, Underbrink JR. Aeroacoustic measurements. 2002.
33. Merino-Martinez R, Snellen M, Simons DG. Functional beamforming applied to full scale landing aircraft. In: 6th Berlin Beamforming Conference. 2016.
34. Dougherty R. Functional beamforming for aeroacoustic source distributions. In: 20th AIAA/CEAS Aeroacoustics Conference. 2014. https://doi.org/10.2514/6.2014-3066.
35. Stoica P, Wang Z, Li J. Robust capon beamforming. IEEE Signal Process Lett. 2003;10(6):172–5. https://doi.org/10.1109/LSP.2003.811637.
36. Sijtsma P. Clean based on spatial source coherence. Int J Aeroacoust. 2007;6(4):357–74. https://doi.org/10.1260/147547207783359459.
37. Brooks TF, Humphreys WMA. deconvolution approach for the mapping of acoustic sources (DAMAS) determined from phased microphone arrays. J Sound Vib. 2006;294(4–5):856–79. https://doi.org/10.1016/j.jsv.2005.12.046.
38. Gupta P, Kar SP. Music and improved music algorithm to estimate direction of arrival. In: 2015 International Conference on Communications and Signal Processing (ICCSP). Melmaruvathur, India; 2015. p. 757–61. https://doi.org/10.1109/ICCSP.2015.7322593.
39. Hald J. Basic theory and properties of statistically optimized near-field acoustical holography. J Acoust Soc Am. 2009;125(4):2105–20. https://doi.org/10.1121/1.3079773.
40. Sijtsma P. Experimental techniques for identification and characterization of noise sources. 2004.
41. Petrica L. An evaluation of low-power microphone array sound source localization for deforestation detection. Appl Acoust. 2016;113:162–9. https://doi.org/10.1016/j.apacoust.2016.06.022.
42. Ramos ALL, Holm S, Gudvangen S, Otterlei R. Delay-and-sum beamforming for direction of arrival estimation applied to gunshot acoustics. In: Proceedings of SPIE - The International Society for Optical Engineering. 2011:8019. https://doi.org/10.1117/12.886833.
43. Moradshahi P, Chatrzarrin H, Goubran R. Cough sound discrimination in noisy environments using microphone array. Conf Rec - IEEE Instrument Measure Technol Conf. 2013;431–4. https://doi.org/10.1109/I2MTC.2013.6555454.
44. Modir Shanechi M, Aarabi P. Structural analysis of multisensor arrays for speech separation applications. Proc SPIE - Int Soc Opt Eng. 2003;5099:327–34. https://doi.org/10.1117/12.488093.
45. Wajid M, Kumar B, Goel A, Kumar A, Bahl R. Direction of arrival estimation with uniform linear array based on recurrent neural network. Proc IEEE Int Conf Signal Process Comput Control. 2019;361–5. https://doi.org/10.1109/ISPCC48220.2019.8988399.
46. Gur B. Particle velocity gradient based acoustic mode beamforming for short linear vector sensor arrays. J Acoust Soc Am. 2014;135(6):3463–73. https://doi.org/10.1121/1.4876180.
47. Koop L, Ehrenfried K. Microphone-array processing for wind-tunnel measurements with strong background noise. In: 14th AIAA/CEAS Aeroacoustics Conference (29th AIAA Aeroacoustics Conference). 2008. https://doi.org/10.2514/6.2008-2907.
48. Ocker C, Pannert W. Imaging of broadband noise from rotating sources in uniform axial flow. In: 22nd AIAA/CEAS Aeroacoustics Conference, 2016. 2016. https://doi.org/10.2514/6.2016-2899.
49. Kim S-M, Byun S-H, Kim K, Choi H-T, Lee C-M. Development and performance test of an underwater sound transmission system for an ROV. In: 2017 IEEE OES International Symposium on Underwater Technology, UT 2017. 2017. https://doi.org/10.1109/UT.2017.7890295.
50. De Araujo FH, Pinto FADNC. Comparison between the spherical harmonics beamforming and the delay-and-sum beamforming. In: Proceedings of the INTER-NOISE 2016 - 45th International Congress and Exposition on Noise Control Engineering: Towards a Quieter Future. 2016. p. 277–87.
51. Tiana-Roig E, Jacobsen F, Fernandez-Grande E. Beamforming with a circular array of microphones mounted on a rigid sphere (l). J Acoust Soc Am. 2011;130(3):1095–8. https://doi.org/10.1121/1.3621294.
52. Kerscher M, Heilmann G, Puhle C, Krause R, Friebe C. Sound source localization on a fast rotating fan using rotational beamforming. In: INTER-NOISE 2017 - 46th International Congress and Exposition on Noise Control Engineering: Taming Noise and Moving Quiet. 2017.
53. Yang Y, Chu Z, Shen L, Xu Z. Functional delay and sum beamforming for three-dimensional acoustic source identification with solid spherical arrays. J Sound Vib. 2016;373:340–59. https://doi.org/10.1016/j.jsv.2016.03.024.
54. Li Y, Ho KC, Popescu M. Efficient source separation algorithms for acoustic fall detection using a microsoft kinect. IEEE Trans Biomed Eng. 2014;61(3):745–55. https://doi.org/10.1109/TBME.2013.2288783.
55. Talmon R, Cohen I, Gannot S. Multichannel speech enhancement using convolutive transfer function approximation in reverberant environments. In: ICASSP, IEEE International Conference on Acoustics, Speech and Signal Processing - Proceedings. 2009. p. 3885–8. https://doi.org/10.1109/ICASSP.2009.4960476.
56. Xia H-J, Ma Y-L, Liu Y-X. Analysis of the symmetry of the ambient noise and study of the noise reduction. Wuli Xuebao/Acta Phys Sin. 2016;65(14). https://doi.org/10.7498/aps.65.144302.
57. Salom I, Celebic V, Milanovic M, Todorovic D, Prezelj J. An implementation of beamforming algorithm on FPGA platform with digital microphone array. 138th Audio Eng Soc Conv. 2015;2:995–1004.
58. Bai L, Huang X. Observer-based beamforming algorithm for acoustic array signal processing. J Acoust Soc Am. 2011;130(6):3803–11. https://doi.org/10.1121/1.3658448.
59. Lashi D, Quévy Q, Lemeire J. Optimizing microphone arrays for delay-and-sum beamforming using genetic algorithms. In: 2018 4th International Conference on Cloud Computing Technologies and Applications, Cloudtech. 2018. https://doi.org/10.1109/CloudTech.2018.8713331.
60. Lauterbach A, Ehrenfried K, Koop L, Loose S. Procedure for the accurate phase calibration of a microphone array. In: 15th AIAA/CEAS Aeroacoustics Conference (30th AIAA Aeroacoustics Conference). 2009. https://doi.org/10.2514/6.2009-3122.
61. Kates JM. Evaluation of hearing-aid array processing. IEEE ASSP Workshop Appl Signal Process Audio Acoust. 1995;4. https://doi.org/10.1109/ASPAA.1995.482902.
62. Yardibi T, Bahr C, Zawodny N, Liu F, Cattafesta LN III, Li J. Uncertainty analysis of the standard delay-and-sum beamformer and array calibration. J Sound Vib. 2010;329(13):2654–82. https://doi.org/10.1016/j.jsv.2010.01.014.
63. Malgoezar A, Snellen M, Simons D, Sijtsma P. Using global optimization methods for acoustic source localization. In: ICSV 2016 - 23rd International Congress on Sound and Vibration: From Ancient to Modern Acoustics. 2016.
64. Chu Z, Yang Y, Shen L. Resolution and quantification accuracy enhancement of functional delay and sum beamforming

for three-dimensional acoustic source identification with solid spherical arrays. Mech Syst Signal Process. 2017;88:274–89. https://doi.org/10.1016/j.ymssp.2016.11.027.
65. Juricka M. Acoustic camera scanning as a detection of noise sources on small aircraft. Acta Avionica J. 2020;12–20. https://doi.org/10.35116/aa.2020.0002.
66. Howell GP, Bradley AJ, McCormick MA, Brown JD. De-dopplerization and acoustic imaging of aircraft flyover noise measurements. J Sound Vib. 1986;105(1):151–67. https://doi.org/10.1016/0022-460X(86)90227-0.
67. Bi Y, Feng X, Zhang Y. Optimized sonar broadband focused beamforming algorithm. Algorithms. 2019;12(2). https://doi.org/10.3390/a12020033.
68. Bi Y, Wang Y-M, Wang Q. Research on dual optimized broadband beamforming algorithm. Binggong Xuebao/Acta Armamentarii. 2017;38(8):1563–71. https://doi.org/10.3969/j.issn.1000-1093.2017.08.014.
69. Bao C, Jia L, Pan J. Use of robust capon beamformer for extracting audio signals. In: Acoustics 2019, Sound Decisions: Moving Forward with Acoustics - Proceedings of the Annual Conference of the Australian Acoustical Society. 2020.
70. Somasundaram SD, Parsons NH. Evaluation of robust capon beamforming for passive sonar. IEEE J Ocean Eng. 2011;36(4):686–95. https://doi.org/10.1109/JOE.2011.2167374.
71. Li J, Stoica P, Wang Z. On robust capon beamforming and diagonal loading. IEEE Trans Signal Process. 2003;51(7):1702–15. https://doi.org/10.1109/TSP.2003.812831.
72. Bao C. Performance of time domain and time-frequency domain adaptive beamformers with moving sound sources. INTERNOISE 2014 - 43rd International Congress on Noise Control Engineering: Improving the World Through Noise Control. 2014.
73. Frost OL. An algorithm for linearly constrained adaptive array processing. Proc IEEE. 1972;60(8):926–35. https://doi.org/10.1109/PROC.1972.8817.
74. Azimi-Sadjadi MR, Pezeshki A, Scharf LL, Hohil ME. Wideband DOA estimation algorithms for multiple target detection and tracking using unattended acoustic sensors. 2004.
75. Camargo HE, Burdisso RA, Ravetta PA, Smith AK. A comparison of beamforming processing techniques for low frequency noise source identification in mining equipment. ASME Int Mech Eng Congr Exposition Proc. 2010;15:205–11. https://doi.org/10.1115/IMECE2009-12194.
76. Rindal OMH, Austeng A, Fatemi A, Rodriguez-Molares A. The effect of dynamic range alterations in the estimation of contrast. IEEE Trans Ultrason Ferroelectr Freq Control. 2019;66(7):1198–208. https://doi.org/10.1109/TUFFC.2019.2911267.
77. He Y, Dong G, Zhang T, Wang B, Shen Z. A study on the correlation between vehicles interior noise and exterior aerodynamic noise sources. 2017;39(10):1192–7. https://doi.org/10.19562/j.chinasae.qcgc.2017.10.015.
78. Chu Z, Zhao S, Yang Y, Yang Y. Deconvolution using clean-sc for acoustic source identification with spherical microphone arrays. J Sound Vib. 2019;440:161–73. https://doi.org/10.1016/j.jsv.2018.10.030.
79. Wang Y, Yang C, Wang Y, Hu D. Fast deconvolution algorithm based on compressed focus grid points. Zhendong yu Chongji/J Vib Shock. 2022;41(6):250–5. https://doi.org/10.13465/j.cnki.jvs.2022.06.032.
80. Legg M, Bradley S. Automatic 3D scanning surface generation for microphone array acoustic imaging. 2014;76:230–7. https://doi.org/10.1016/j.apacoust.2013.08.008.
81. Baali H, Bouzerdoum A, Khelif A. Sparsity and nonnegativity constrained Krylov approach for direction of arrival estimation. ICASSP IEEE Int Conf Acoust Speech Signal Process - Proc. 2021;2021:4400–4. https://doi.org/10.1109/ICASSP39728.2021.9415040.
82. Wu Y, He Y, Shen Z, Yang Z. Application of improved beamforming algorithm in sound source identification at wind tunnel. Tongji Daxue Xuebao/J Tongji Univ. 2019;47:20–5. https://doi.org/10.11908/j.issn.0253-374x.19707.
83. Ma W, Liu X. Compression computational grid based on functional beamforming for acoustic source localization. Appl Acoust. 2018;134:75–87. https://doi.org/10.1016/j.apacoust.2018.01.006.
84. Ravetta P, Burdisso R. Noise source localization and optimization of phased array results (lore). AIAA J. 2006;47. https://doi.org/10.2514/6.2006-2713.
85. Ravetta P, Burdisso R, Ng W, Sijtsma P, Stoker R, Underbrink J, Dougherty R, Khorrami M. Noise source localization and optimization of phased-array results. AIAA J. 2009;47:2520–33. https://doi.org/10.2514/1.38073.
86. Qayyum H, Ashraf M. Performance comparison of direction-of-arrival estimation algorithms for towed array sonar system. Commun Comput Info Sci. 2011;189(CCIS(PART 2)):509–17 . https://doi.org/10.1007/978-3-642-22410-2_44.
87. Benesty J, Chen J, Huang Y. A generalized MVDR spectrum. Signal Process Lett IEEE. 2006;12:827–30. https://doi.org/10.1109/LSP.2005.859517.
88. Defatta DJJGL, Hodkiss WS. Digital signal processing a system approach. 1st Edition. Wiley; 1988.
89. Moallemi N, ShahbazPanahi S. Immersion ultrasonic array imaging using a new array spatial signature in different imaging algorithms. Conf Rec - Asilomar Conf Signals Syst Comput. 2014;2015:1558–61. https://doi.org/10.1109/ACSSC.2014.7094726.
90. Sun JC, Shin CW, Ju HJ, Paik SK, Kang YJ. Measurement of the normal acoustic impedance using beamforming method. J Mech Sci Technol. 2009;23(8):2169–78. https://doi.org/10.1007/s12206-009-0435-z.
91. Swingler DN, Walker RS. Line-array beamforming using linear prediction for aperture interpolation and extrapolation. IEEE Trans Acoust Speech Signal Process. 1989;37(1):16–30. https://doi.org/10.1109/29.17497.
92. Liu C, Lv Y, Miao J, Shang H. Research on high resolution algorithm of sound source localization based on microphone array. In: ICSIDP 2019 - IEEE International Conference on Signal, Information and Data Processing. 2019. https://doi.org/10.1109/ICSIDP47821.2019.9173224.
93. Zhang Y, Chen J, Zhou N, Luo L, Sheng G. Joint acoustic source localization algorithm based on summation and music algorithm for power equipment in substations. Proc - 2020 5th Asia Conf Power Electr Eng, ACPEE 2020. 2020. p. 26–31. https://doi.org/10.1109/ACPEE48638.2020.9136575.
94. Fan W, Zhang X, Jiang B. A new passive sonar bearing estimation algorithm combined with blind source separation. In: 3rd International Joint Conference on Computational Sciences and Optimization, CSO 2010: Theoretical Development and Engineering Practice, vol. 1, 2010. p. 15–8. https://doi.org/10.1109/CSO.2010.201.
95. Kassis C, Picheral J. Wideband zero-forcing music for aeroacoustic sources localization. Eur Signal Process Conf. 2012;2283–7.
96. Xiao H, Shao H-Z, Peng Q-C. A robust sound source localization approach for microphone array with model errors. IEICE Trans Fundamentals Electron Commun Comput Sci. 2008;E91–A(8):2062–7. https://doi.org/10.1093/ietfec/e91-a.8.2062.
97. Sheikh MA, Kumar L, Beg MT. Circular microphone array based stethoscope for radial filtering of body sounds. In: 2019 International Conference on Power Electronics, Control and Automation, ICPECA 2019 - Proceedings. 2019. https://doi.org/10.1109/ICPECA47973.2019.8975663.

98. Bai MR, Lee J. Industrial noise source identification by using an acoustic beamforming system. J Vib Acoust Trans ASME. 1998;120(2):426–33. https://doi.org/10.1115/1.2893847.